

Copyright Warning & Restrictions

The copyright law of the United States (Title 17, United States Code) governs the making of photocopies or other reproductions of copyrighted material.

Under certain conditions specified in the law, libraries and archives are authorized to furnish a photocopy or other reproduction. One of these specified conditions is that the photocopy or reproduction is not to be “used for any purpose other than private study, scholarship, or research.” If a user makes a request for, or later uses, a photocopy or reproduction for purposes in excess of “fair use” that user may be liable for copyright infringement,

This institution reserves the right to refuse to accept a copying order if, in its judgment, fulfillment of the order would involve violation of copyright law.

Please Note: The author retains the copyright while the New Jersey Institute of Technology reserves the right to distribute this thesis or dissertation

Printing note: If you do not wish to print this page, then select “Pages from: first page # to: last page #” on the print dialog screen

The Van Houten library has removed some of the personal information and all signatures from the approval page and biographical sketches of theses and dissertations in order to protect the identity of NJIT graduates and faculty.

ABSTRACT

KOH ETCHING OF SILICON

by
Ying Wang

In this research, a series of comparative etching experiments on silicon wafers have been carried out using potassium hydroxide (KOH) for different experimental etching conditions for concentration, temperature and time on (100) orientation p-type silicon wafers. Besides the basic etching conditions, the position of the immersed wafer also has unpredictable effect on the etching process. This may be attributed to the relative contact position between the surface of the immersed wafer and the flow patterns of the stirred etching solution.

The surface morphology analysis indicates that the specific position of the wafer, with respect to the flow of the etchant, can lead to a higher quality of uniformly rough (100) crystal face. The lowest reflectivity of etched sample is determined by using reflectivity measurements. The study reveals that, besides conventional etching conditions, the etching positions, which can be easily disregarded, are also potential conditions that have significant influence on the etching results; this may become a principal condition for etching of silicon by KOH.

KOH ETCHING OF SILICON

**by
Ying Wang**

**A Thesis
Submitted to the Faculty of
New Jersey Institute of Technology
in Partial Fulfillment of the Requirements for the Degree of
Master of Science in Materials Science and Engineering
Interdisciplinary Program in Materials Science and Engineering
May 2016**

Blank Page

APPROVAL PAGE
KOH ETCHING OF SILICON
Ying Wang

Dr. N. M. Ravindra, Professor of Physics, NJIT Director of Interdisciplinary Program in Materials Science and Engineering, NJIT	Date
---	------

Dr. Angelo Perna, Committee Member Professor of Chemical, Biological & Pharmaceutical Engineering, NJIT	Date
--	------

Dr. Edip Niver, Committee Member Professor of Electrical & Computer Engineering, NJIT	Date
--	------

BIOGRAPHICAL SKETCH

Author: Ying Wang

Degree: Master of Science

Date: May 2016

Undergraduate and Graduate Education:

- Master of Material Science and Engineering,
New Jersey Institute of Technology, Newark, NJ, 2016
- Bachelor of Inorganic Non-metallic Material Engineering,
Dalian University of Technology, Dalian, P. R. China, 2013

Major: Materials Science and Engineering

This thesis is dedicated to my parents who supported me to finish my study and to my advisors who helped me a lot during the thesis, and finally in memory of my deceased maternal grandfather.

ACKNOWLEDGMENT

I would like to thank my thesis advisors Dr. Oktay H Gokce and Dr. N. M. Ravindra for their great kindness and help throughout my thesis. I would also like to thank my committee members: Dr. Angelo Perna and Dr. Edip Niver for their support and encouragement.

I thank Dr. Benchafia El Mostafa and Dr. George E. Georgiou for providing help with characterization.

I also appreciate Mr. Yogesh Gandhi for providing supplies.

I thank Mr. Scott Sanowitz for helping me with reflectivity analyses.

I am thankful to Y.Y. Wen and P. Lin, two of my friends who majored in Physics, for helping me to analyze the mechanics of fluids.

And last but not least, my special thanks to my parents for their great love and support, my deceased maternal grandfather for his inspiring encouragement.

TABLE OF CONTENTS

Chapter	Page
1 INTRODUCTION.....	1
1.1 Objective	1
1.2 Background Information	2
1.3 Applications.....	4
2 REVIEW OF LITERATURE.....	7
2.1 Characteristics of KOH Etching.....	7
2.2 Differences between Wet Etching and Dry Etching.....	8
2.3 Differences between Anisotropic Etching and Isotropic Etching.....	11
2.4 Definition of Undercut.....	13
2.5 Related Characterization.....	14
2.6 Fundamental Knowledge of Fluid Mechanics.....	19
3 EXPERIMENTAL.....	25
3.1 Research Purpose.....	25
3.2 Substrate.....	25
3.3 Apparatus.....	26
3.4 Procedure.....	27
3.5 Characterization Methods.....	28
4 RESULTS AND DISCUSSION.....	29
4.1 Comparison of Silicon Etch Rates in Different Conditions of KOH Solutions.....	29

TABLE OF CONTENTS
(Continued)

Chapter	Page
4.2 Comparison of Surface Morphologies Etched by Different Conditions of KOH Solutions with Different Immersed Positions.....	35
4.3 Surface Reflectivity Analysis.....	45
5 CONCLUSION.....	48
REFERENCES	50
SUPPLEMENTARY DIAGRAMS.....	55

LIST OF TABLES

Table	Page
2.1 Common Anisotropic Etchants for Silicon.....	8
3.2 Basic Properties of Potassium Hydroxide (KOH).....	25
4.2 Top View of Immersed Positions.....	42
4.3 Reflectivity Measured with Black-Body Infrared Radiation System.....	46

LIST OF FIGURES

Figure	Page
1.1 The difference between etching rates of (100) and (110) orientation.....	3
2.2.1 The plasma hits the silicon wafer with high energy to knock-off the Si atoms on the surface.....	9
2.2.2 Process of a reactive ion interacting with the silicon surface.....	10
2.2.3 The RIE process.....	10
2.3 Different results in etching of silicon.....	12
2.4 Simplified schematic diagram of undercut.....	14
2.5.1 Energy-level diagram showing the states involved in Raman signal.....	15
2.5.2 Schematic diagram of FTIR.....	16
2.5.3 Schematic of UV-visible spectroscopy.....	17
2.5.4 Schematic of a SEM.....	19
3.3 Simplified schematic diagram of experimental apparatus.....	27
4.1.1 Raman spectra of samples.....	29
4.1.2 Screenshots of profilometer spectrograms of samples.....	32
4.2.1 SEM images of etched Si surface morphology showing pyramidal and hillock structures.....	37
4.2.2 Photographs of etched samples immersed in different positions.....	40
4.2.3 Optical micrographs of etched samples immersed in different positions.....	41
6.1 Screenshots of profilometer spectrograms of samples.....	54
6.2 SEM images of etched Si surface morphology showing pyramidal and hillock structures.....	55

CHAPTER 1

INTRODUCTION

1.1 Objective

In order to fabricate high-efficiency crystalline Si solar cells, the surface light reflection should be minimized, and the formation of uniformly rough surface of Si decreases the surface reflection substantially. The uniformly rough structure includes random-rough and inverted-rough topographies. Compared with random-rough, inverted-rough is a more efficient single-side light trapping geometry since it has superior internal response coupled with the path length enhancement and reduced front surface reflectance. This can improve short-circuit current in solar cells [1,2].

Wet chemical etching has been extensively used in fabricating silicon microstructures [3]. One example is to use silicon microstructures as a template for the replication of polymer structures in molding and imprinting processes [4]. In molding and imprinting processes, the quality of the template plays a crucial role in replicating the polymer structures because the replication resolution reaches ranges below ten nanometers. Therefore, any unwanted features such as surface roughness of the template should be minimized. Previous works reporting on the dependence of the wet-etched silicon surface roughness on the temperature and concentration of the etchants [5–7] have shown different roughness characteristics in the crystallographic orientation of the silicon surfaces [8,9]. Minimizing the surface roughness of the template is especially important for the formation of polymer replica for optical applications such as waveguides or mirrors to maintain low light scattering loss.

Silicon etching in alkaline solutions has been employed for many years but the mechanism of the process has not been completely recognized yet, especially from the point of view of etching anisotropy, which is associated with various configurations of surface bonds. These bonds have been described in detail and classified in the literature [10-14]. Also, the morphologies and etch rates of Si substrates with different crystallographic orientations, etched in the solutions with different compositions, are commonly known [6,14-16]. However, the connection between the results of etching and the compositions of etching solutions is still under debate. The etching in KOH and TMAH solutions, where the relations among the etch rates of particular planes (so called anisotropy factor) are different, can be a good example. The process becomes more complicated when tensioactive compounds or surfactants are added to the etching solutions.

1.2 Background Information

Inverted-smooth patterns are formed by anisotropic etching of a patterned (1 0 0) Si surface. Alkali metal hydroxides (e.g. KOH or NaOH) are the most common etchants for anisotropic etching of Si [17-19]. However, as the alkaline-based solutions result in the metal ion contamination, which is difficult to remove in the subsequent cleaning [20], it is necessary to study organic alkaline etchants that do not introduce metal ions so that they can be IC-fabrication compatible.

Wet anisotropic etching of silicon substrates is commonly used in micromechanics for the fabrication of different MEMS structures including membranes, “bossed-type” features, suspended beams, seismic masses, etc. In many practical applications, the

problem of control of etched surface morphology is of the greatest importance. The roughness of different silicon crystallographic planes etched in KOH and TMAH solutions have been studied extensively in the last few years. A comprehensive survey of characteristic patterns that are typical for different crystallographic orientations has been delivered by sphere etching experiments [21–23]. Attempts have been undertaken to correlate the etched surface appearance with three main close-packed silicon surfaces and their vicinal [15,24]. There are many simulators for modelling the etched surface morphology and vice versa, examination of different surface morphologies delivers the necessary data for studying site-specific reaction kinetics by Monte Carlo simulations [25,26].

Generally, the quality of etched surface is a complex matter. It depends on many factors like crystallographic orientation of etched substrate, kind of etching solution and its concentration as well as process parameters [15,22,23]. Change in surface morphology with etching time and temperature have been reported [22,23]. It was observed that the change in etchant concentration can have beneficial effect on some planes and deteriorate the quality of the others. For example, it was reported [24] that the increase in KOH concentration results in reduction of hillocks on (100) surface but causes their increase on (110).



Figure 1.1 The difference between etching rates of (100) and (110) orientation.

Source: Ronny Nawrodt, Silicon Surfaces – Silicon Loss and Silicon Treatments –, 1st ELiTES General Meeting, Tokyo, 04/10/2012.

Texturing for crystalline silicon solar cells is one of the major techniques employed to improve the conversion efficiency by increasing the amount of light absorption [27]. Generally, for mono-crystalline silicon, both alkali hydroxide etchants such as potassium hydroxide (KOH) or sodium hydroxide (NaOH) and simple and quaternary ammonium hydroxide etchants, typically tetramethyl ammonium hydroxide (TMAH), are used by mixing them with isopropyl alcohol (IPA), and then these mixed solutions are used to anisotropically etch the silicon, leaving random pyramids on the surface [28-30]. Even though these pyramids improve the short circuit current through effective photon trapping, it is unclear how they affect the other properties.

1.3 Applications

Light management is crucial to solar cell design as it increases the path length of light in the absorber layer, thereby enhancing the probability of electron-hole pair generation. By engineering the reflective and refractive properties of the solar cell surfaces, we can trap light within the active region to achieve physically thin, but optically thick solar cells.

Texturing the surface of solar cells is an effective light management technique, providing both light trapping and anti-reflection properties [31–35]. The operational spectrum of a single-junction silicon solar cell is from 300nm to 1200nm. In the ultraviolet and visible spectrum where the photon energy is well above the bandgap energy of silicon, all light coupled into the Si is absorbed before reaching the rear side of the cell. In contrast, in the near-infrared region, the probability of a band transition of a photon-excited electron reduces significantly. At these wavelengths, surface textures can preferentially direct light

into the solar cell at angles outside the escape cone of silicon, resulting in light trapping and increased absorption.

As solar cell technology becomes increasingly competitive, accurately estimating the light-trapping-induced current enhancement at an early stage of solar cell fabrication is very important. It is therefore highly desirable to have a technique that accurately assesses optical absorption enhancement, with the ability to distinguish between band-to-band absorption and parasitic absorption [36,37]. Conventional methods such as photo-thermal deflection and reflection (R) or transmission (T) measurements ($A=I-R-T$) provide inaccurate estimates of absorption (A) and, hence, photocurrent generation as they inevitably include parasitic absorption [38].

In a solar cell, only photons that excite an electron from the valence band to the conduction band contribute to the photo-current generation. In the inverse process, electron-hole pairs recombine and photons are emitted via band-to-band radiation, which can be directly quantified from the measured photoluminescence (PL) spectrum [37,39–43]. Therefore, by studying the PL spectrum of silicon wafers, we can derive the portion of the absorbed photons that lead to effective electron-hole generation. In a silicon wafer, both carrier densities and the optical properties of the sample determine the PL intensity at a given wavelength. The carrier densities of the sample determine the internal generation rate of emitted photons, while the optical properties determine the probability of a photon escaping the sample and contributing to the measured spectrum [44]. There are a number of studies in the literature that model the spectral distribution of photo/electroluminescence emission of silicon wafers or solar cells [39–42,45]. The relationship between spectral

photo-luminescence intensity per energy interval I_{PL} and band-to-band transition absorptivity can be described as follows [40,41,44]:

$$I_{PL}(\hbar\omega) = C \exp\left(\frac{\varepsilon_{F.C} - \varepsilon_{F.V}}{kT}\right) A_{BB} * (\hbar\omega)^2 \exp\left(-\frac{\hbar\omega}{kT}\right) d(\hbar\omega) \quad (1.1)$$

In equation (1.1), C is a constant of proportionality, $\varepsilon_{F.C} - \varepsilon_{F.V}$ is the difference in the quasi-Fermi energies in the semiconductor, k is the Boltzmann constant, T is temperature in Kelvin, and $\hbar\omega$ is the photon energy. Quantifying the absolute absorptance, A_{BB} , that generates electron-hole pairs in a silicon wafer can provide a quick and accurate estimation of the maximum possible current density J_{sc} in a solar cell without the need for a p-n junction and current extraction. The methods for obtaining the absolute absorptance of silicon solar cells and wafers from electroluminescence spectra and photoluminescence spectra have been experimentally demonstrated by Trupke *et al.* and Barugkin *et al.* [37,40].

CHAPTER 2

REVIEW OF LITERATURE

2.1 Characteristics of KOH Etching

Potassium Hydroxide (KOH) etches silicon wafer at very different rates depending on which crystal face is exposed. In silicon wafers, which is the single-crystal material, this effect can allow very high anisotropy. The term "crystallographic etching" can also be explained as "anisotropic etching along crystal planes".

Potassium hydroxide displays an etch rate selectivity 400 times higher in (100) crystal directions than in (111) directions. It also displays high selectivity between lightly doped and heavily boron-doped (p-type) silicon. KOH may introduce mobile potassium ions into silicon dioxide; therefore, control is required in its use.

Etching a (100) silicon surface through a rectangular hole in a masking material, for example, a hole in a layer of native oxide, creates a pit with flat sloping (111) oriented sidewalls and a flat (100) oriented bottom. The (111) oriented sidewalls have an angle to the surface of the wafer of:

$$\text{arc tan } \sqrt{2} = 54.7^\circ \tag{2.1}$$

If the etching is continued "to completion", i.e. until the flat bottom disappears, the pit becomes a trench with a V-shaped cross section. If the original rectangle was a perfect square, the pit when etched to completion displays a pyramidal shape.

The undercut, δ , under an edge of the masking material is given by:

$$\delta = \frac{\sqrt{6}D}{S} = \frac{\sqrt{6}R_{100} T}{R_{100} / R_{111}} = \sqrt{6}TR_{111} \quad (2.2)$$

where R_{xxx} is the etch rate in the $\langle xxx \rangle$ direction, T is the etch time, D is the etch depth and S is the anisotropy of the material and etchant. Different etchants have different anisotropies. Table 2.1 presents a table of common anisotropic etchants for silicon:

Table 2.1 Common Anisotropic Etchants for Silicon

Etchant	Operating temp (°C)	R_{100} ($\mu\text{m}/\text{min}$)	$S=R_{100}/R_{111}$	Mask materials
Ethylenediamine pyrocatechol (EDP)	110	0.47	17	SiO_2 , Si_3N_4 , Au, Cr, Ag, Cu
Potassium hydroxide/Isopropyl alcohol (KOH/IPA)	50	1.0	400	Si_3N_4 , SiO_2 (etches at 2.8 nm/min)
Tetramethylammonium hydroxide (TMAH)	80	0.6	37	Si_3N_4 , SiO_2

Source: [https://en.wikipedia.org/wiki/Etching_\(microfabrication\)](https://en.wikipedia.org/wiki/Etching_(microfabrication)).

2.2 Differences between Wet Etching and Dry Etching

Wet etching is a material removal process that uses liquid chemicals or etchants to remove materials from a wafer. The specific patterns are defined by masks on the wafer. Materials that are not protected by the masks are etched away by liquid chemicals. These masks are deposited and patterned on the wafers in a prior fabrication step using lithography.

A wet etching process involves multiple chemical reactions that consume the original reactants and produce new reactants. The wet etch process can be described by three basic steps: (1) Diffusion of the liquid etchant to the structure that is to be removed; (2) The reaction between the liquid etchant and the material being etched away. A

reduction-oxidation (redox) reaction usually occurs. This reaction entails the oxidation of the material and then dissolving the oxidized material. (3) Diffusion of the byproducts in the reaction from the reacted surface.

On the other hand, in dry etching, plasmas or etchant gasses remove the substrate material. The reaction that takes place can be done by utilizing high kinetic energy of particle beams, chemical reaction or a combination of both.

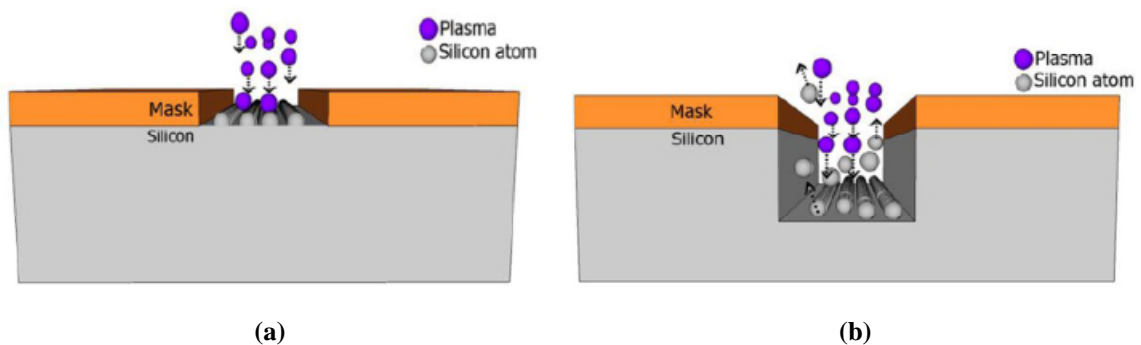


Figure 2.2.1 The plasma hits the silicon wafer with high energy to knock-off the Si atoms on the surface. (a) The plasma atoms hitting the surface. (b) The silicon atoms being evaporated off from the surface.

Source: Wet and Dry Etching Avinash P. Nayak, Logeeswaran VJ and M. Saif Islam† University of California, Davis. California.

Dry etching includes the removal of the material, typically a masked pattern of semiconductor material, by exposing the material to a bombardment of ions (usually a plasma of reactive gases, such as fluorocarbons, oxygen, chlorine, boron trichloride, sometimes with addition of nitrogen, argon, helium and other gases) that dislodge portions of the material from the exposed surface.

Physical dry etching requires high energy (kinetic energy of ion, electron, or photon) beams to etch off the substrate atoms. When the high-energy particles knock out the atoms from the substrate surface, the material evaporates after leaving the substrate. There is no chemical reaction taking place and therefore only the material that is unmasked will be removed.

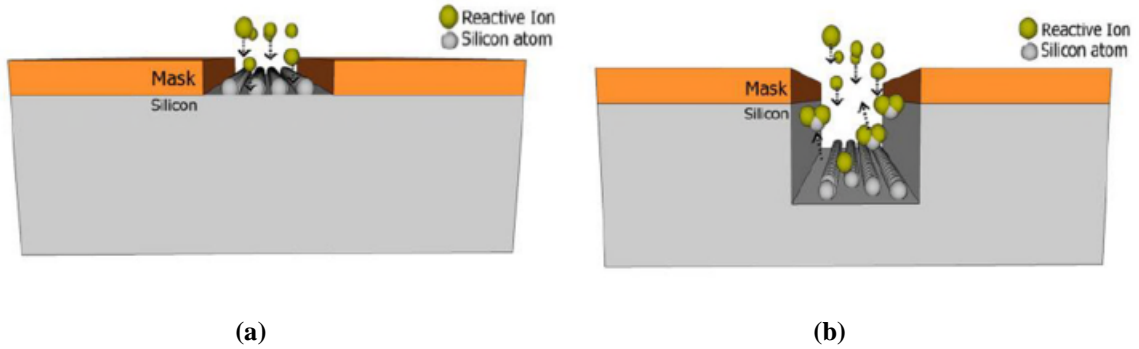


Figure 2.2.2 Process of a reactive ion interacting with the silicon surface. (a) The interaction between the reactive ion and the silicon atom. (b) A bond between the reactive ion and the silicon atom then chemically removes the silicon atoms from the surface.

Source: Wet and Dry Etching Avinash P. Nayak, Logeeswaran VJ and M. Saif Islam† University of California, Davis. California.

Chemical dry etching (also called vapor phase etching) does not use liquid chemicals or etchants. This process involves a chemical reaction between etchant gases and the silicon surface. The chemical dry etching process is usually isotropic and exhibits high selectivity. Anisotropic dry etching has the ability to etch with finer resolution and higher aspect ratio than isotropic etching. Due to the directional nature of dry etching, undercutting can be avoided.

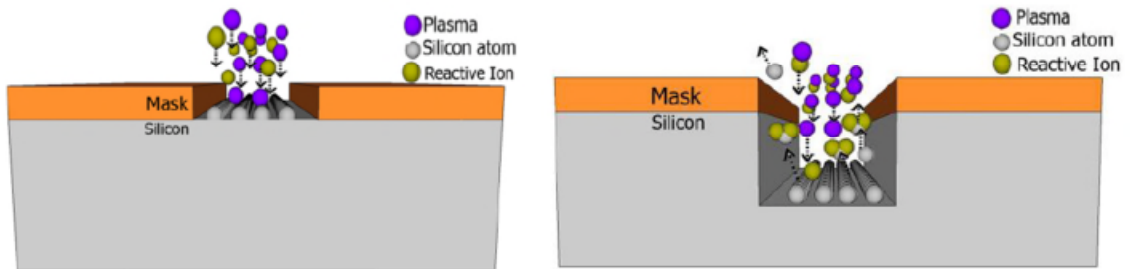


Figure 2.2.3 The RIE process. This process involves both physical and chemical reactions to etch off the silicon.

Source: Wet and Dry Etching Avinash P. Nayak, Logeeswaran VJ and M. Saif Islam† University of California, Davis. California.

Reactive ion etching (RIE) uses both physical and chemical mechanisms to achieve high levels of resolution. The process is one of the most diverse and most widely used

process in industry and research. Since the process combines both physical and chemical interactions, it is much faster. The high energy collision from the ionization helps to dissociate the etchant molecules into more reactive species. In the RIE-process, cations are produced from the reactive gases which are accelerated with high energy to the substrate and chemically react with the silicon. The typical RIE gasses for Si are CF_4 , SF_6 and BCl_2+Cl_2 .

2.3 Differences between Anisotropic Etching and Isotropic Etching

When a material is attacked by a liquid or vapor etchant, it is removed isotropically (uniformly in all directions) or anisotropically (uniformity in vertical direction). The difference between isotropic etching and anisotropic etching is shown in Figure 2.3. Material removal rate for wet-etching is usually faster than the rates for many dry etching processes and can easily be changed by varying temperature or the concentration of active species.

In general, chemical wet etching process after pre-treatment, such as pattern formation, is taking place on the substrate; the next step is to etch the substrate to obtain certain surface structure. Based on the etching shape, the methods can be divided into two kinds, one is isotropic etching with round shape, and the other is anisotropic etching with sharp features.

Isotropic etching is an etching method which removes part of the substrate non-directionally (Fig 2.3(a)), resulting in round corners. On the contrary, anisotropic etching means each crystallographic orientation has different etching rates; so the corners are sharp (Fig 2.3(b), (c)).The etching corners of isotropic etching (Fig 2.3(a)) are round,

and the etching rates of each planes are the same. The shape of anisotropic etching of (100) oriented silicon is an isosceles with a base angle of 54.74° (Fig 2.3(b)). For anisotropic etched (110) oriented silicon wafers (Fig 2.3(c)), U-shaped grooves tend to form.

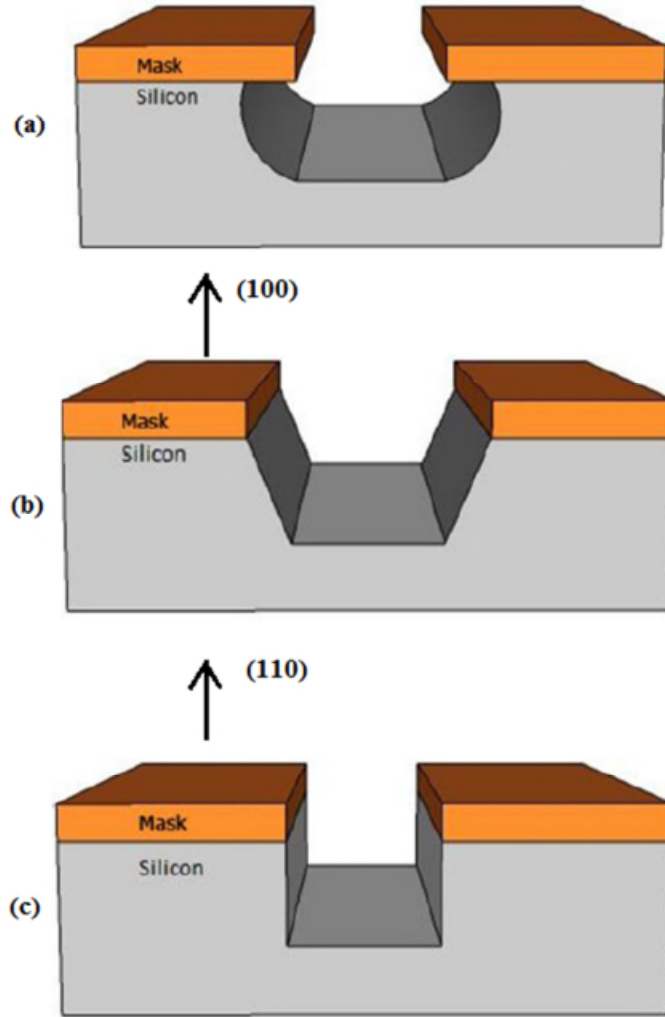


Figure 2.3 Different results in etching of silicon. (a) Isotropic Etching of silicon; (b) Anisotropic Etching of (100) silicon; (c) Anisotropic Etching of (110) silicon.

Source: Wet and Dry Etching Avinash P. Nayak, Logeeswaran VJ and M. Saif Islam† University of California, Davis. California.

As the most commonly used etchant for isotropic etching solution in silicon etching, the HNA solution is a mixture of hydrofluoric acid (HF), nitric acid (HNO_3) and acetic acid (CH_3COOH) [46]. The overall reaction is as follows:

(2.3)



The reaction is a two-step process. At the beginning, silicon substrate is oxidized by HNO_3 . After that, fluoride ions from HF solution form the soluble silicon compound H_2SiF_6 . The next step is to use acetic acid to prevent the dissociation of HNO_3 .

Due to the different etching rates in different silicon planes, anisotropic etching of silicon is often used for making complex shapes, such as V-shaped grooves, U-shaped grooves, pyramidal pits, and pyramidal cavities. The orientation of the silicon wafer and the shape of the mask pattern determine the final etched shape. Most anisotropic etchants for silicon are alkaline solutions and have the same overall reaction:



Directional wet etching of silicon is well developed for applications in microelectronics. Notable etchants include potassium hydroxide (KOH), ethylene diaminepyrocatechol (EDP), and tetramethyl ammonium hydroxide (TMAH)

2.4 Definition of Undercut

In manufacturing, an undercut is a special type of recessed surface. In turning, it refers to a recess in a diameter. In machining, it refers to a recess in a corner. In molding, it refers to a feature that cannot be molded using only a single pull mold. In printed circuit board construction, it refers to the portion of the copper that is etched away under the photoresist. In welding, it refers to undesired melting and removal of metal near the weld bead.

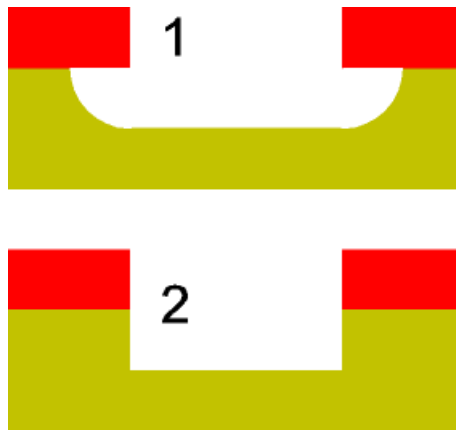


Figure 2.4 Simplified schematic diagram of undercut

1. An isotropic etchant that creates an undercut; 2. An anisotropic etchant leaves no undercut.

Source: https://upload.wikimedia.org/wikipedia/commons/7/72/Etch_anisotropy.png

Also, undercuts from etching are somewhat different from the undercuts explained above, because it is a side effect, not an intentional feature. Undercuts from etching can occur from two common causes. The first is over etching, which means the etchant was applied too long. The second is due to an isotropic etchant, which means the etchant etches in all directions equally. To overcome this problem, an anisotropic etchant is used.

2.5 Related Characterization

Raman Spectroscopy

Raman spectroscopy is a spectroscopic technique used to observe vibrational, rotational, and other low-frequency modes in a system. Raman spectroscopy is commonly used in chemistry to provide a fingerprint by which the molecules can be identified.

It relies on inelastic scattering, or Raman scattering, of monochromatic light, usually from a laser in the visible, near infrared, or near ultraviolet range. The laser light interacts with molecular vibrations, phonons or other excitations in the system, resulting in the

energy of the laser photons being shifted up or down. The shift in energy gives information regarding the vibrational modes in the system. Infrared spectroscopy yields similar, but complementary, information.

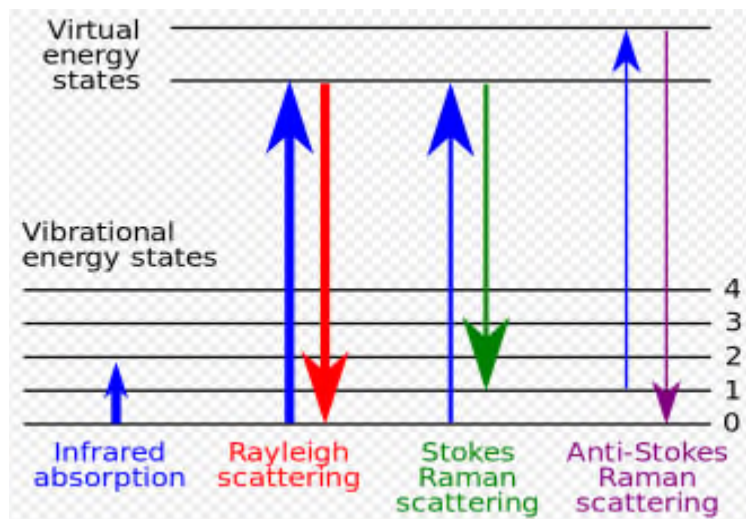


Figure 2.5.1 Energy-level diagram showing the states involved in Raman signal. The line thickness is roughly proportional to the signal strength from the different transitions.

Source: https://upload.wikimedia.org/wikipedia/commons/4/41/Raman_energy_levels.svg

Typically, a sample is illuminated with a laser beam. Electromagnetic radiation from the illuminated spot is collected with a lens and sent through a monochromator. Elastic scattered radiation at the wavelength corresponding to the laser line (Rayleigh scattering) is filtered out, while the rest of the collected light is dispersed onto a detector by either a notch filter or a band pass filter.

FTIR

Fourier transform infrared spectroscopy (FTIR) is a technique which is used to obtain an infrared spectrum of absorption or emission of a solid, liquid or gas. An FTIR spectrometer simultaneously collects high spectral resolution data over a wide spectral range. This confers a significant advantage over a dispersive spectrometer which measures intensity over a narrow range of wavelengths at a time.

The term Fourier transform infrared spectroscopy originates from the fact that a Fourier transform (a mathematical process) is required to convert the raw data into the actual spectrum.

The Fourier transform deconvolutes a signal (a function of time) into the frequencies that constitute the signal. The Fourier transform of a function of time itself is a complex-valued function of frequency, whose absolute value represents the amount of that frequency present in the original function, and whose complex argument is the phase offset of the basic sinusoid in that frequency. The Fourier transform is called the frequency domain representation of the original signal. The term Fourier transform refers to both the frequency domain representation and the mathematical operation that associates the frequency domain representation to a function of time. The Fourier transform is not limited to functions of time, but in order to have a unified language, the domain of the original function is commonly referred to as the time domain.

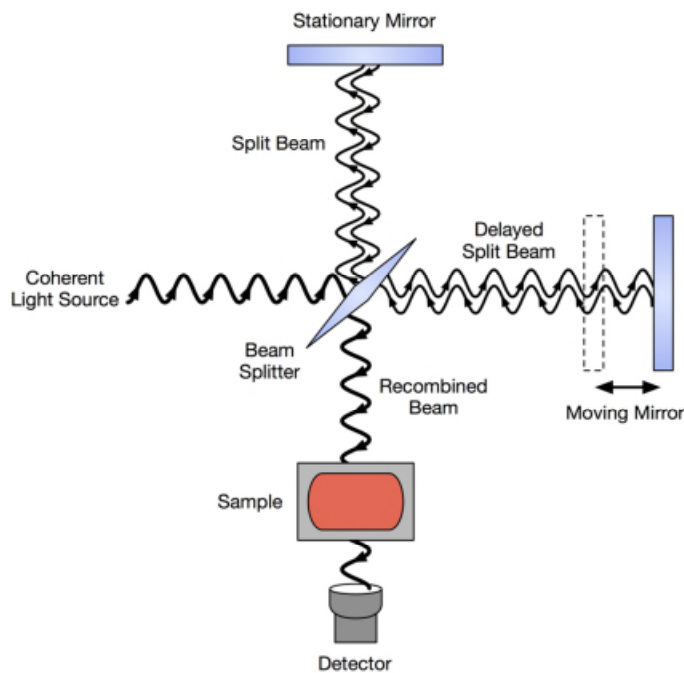


Figure 2.5.2 Schematic diagram of a FTIR.

Source: https://upload.wikimedia.org/wikipedia/commons/a/a1/FTIR_Interferometer.png

UV-VIS-NIR

A Ultraviolet-visible-near-infrared spectroscopy (UV-VIS-NIR) refers to absorption spectroscopy or reflectance spectroscopy in the ultraviolet-visible spectral region. This means it uses light in the visible and adjacent (near-UV and near-infrared [NIR]) ranges. The absorption or reflectance in the visible range directly affects the perceived color of the chemicals involved. In this region of the electromagnetic spectrum, molecules undergo electronic transitions. This technique is complementary to fluorescence spectroscopy, in that fluorescence deals with transitions from the excited state to the ground state, while absorption measures transitions from the ground state to the excited state.

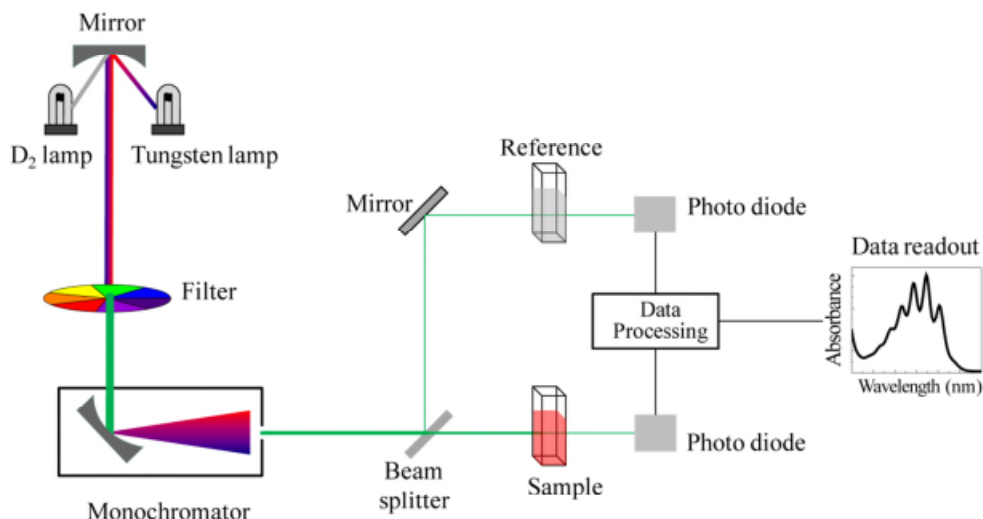


Figure 2.5.3 Schematic of UV- visible spectrophotometer.

Source: https://upload.wikimedia.org/wikipedia/commons/9/95/Schematic_of_UV-_visible_spectrophotometer.png.

Black-Body Infrared Radiation System

The infrared detector used in measuring infrared radiation was from © FLIR[®] Systems, Inc.

The two main types of detectors are thermal and photonic (photodetectors).

The thermal effects of the incident IR radiation can be followed through many temperature dependent phenomena. Bolometers and microbolometers are based on changes in resistance. Thermocouples and thermopiles use the thermoelectric effect. Golay cells follow thermal expansion. In IR spectrometers, the pyroelectric detectors are the most widespread. The response time and sensitivity of photonic detectors can be much higher, but usually these have to be cooled to reduce thermal noise. The materials in these are semiconductors with narrow band gaps. Incident IR photons can cause electronic excitations. In photoconductive detectors, the resistivity of the detector element is monitored. Photovoltaic detectors contain a p-n junction on which photoelectric current appears upon illumination.

SEM

A scanning electron microscope (SEM) is a type of electron microscope that produces images of a sample by scanning it with a focused beam of electrons. The electrons interact with atoms in the sample, producing various signals that contain information about the sample's surface, topography and composition. The electron beam is generally scanned in a raster scan pattern, and the beam's position is combined with the detected signal to produce an image. SEM can achieve resolution better than 1 nanometer. Specimens can be observed in high vacuum, in low vacuum, in wet conditions (in environmental SEM), and at a wide range of cryogenic or elevated temperatures.

The most common SEM mode is detection of secondary electrons emitted by atoms excited by the electron beam. The number of secondary electrons that can be detected depends, among other things, on the angle at which the beam meets the surface of the specimen, i.e. on specimen topography. By scanning the sample and collecting the

secondary electrons that are emitted using a special detector, an image displaying the topography of the surface is created.

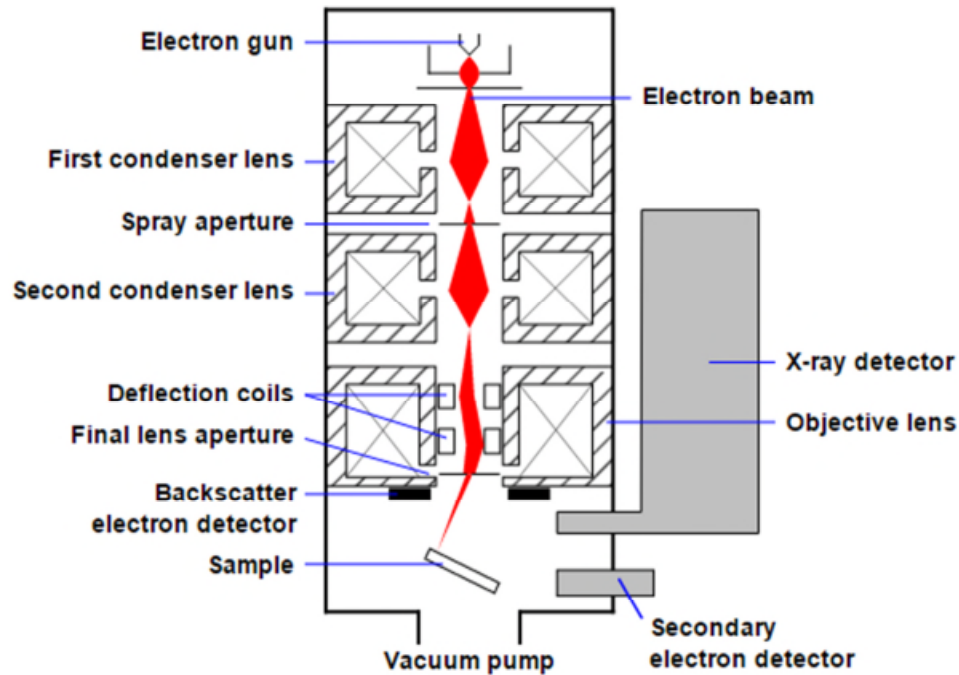


Figure 2.5.4 Schematic of SEM.

Source: https://upload.wikimedia.org/wikipedia/commons/0/0d/Schema_MEB_%28en%29.svg

2.6 Fundamental Knowledge of Fluid Mechanics

Flow Field and Flow Lines

Flow field is a kind of occupied space when fluid flows.

In a flow field, fluid flow is characterized by a velocity vector field in three-dimensional space, within the framework of continuum mechanics. Streamlines, streaklines, and pathlines are field lines resulting from this vector field description of the flow. They differ only when the flow changes with time: that is, when the flow is not steady.

(1) **Streamlines** are a family of curves that are instantaneously tangent to the velocity vector of the flow. These show the direction that a massless fluid element will travel at any point in time.

(2) **Streaklines** are the loci of points of all the fluid particles that have passed continuously through a particular spatial point in the past. Dye steadily injected into the fluid at a fixed point extends along a streakline.

(3) **Pathlines** are the trajectories that individual fluid particles follow. These can be thought of as "recording" the path of a fluid element in the flow over a certain period. The direction the path takes will be determined by the streamlines of the fluid at each moment in time.

(4) **Timelines** are the lines formed by a set of fluid particles that are marked at a previous instant in time, creating a line or a curve that is displaced in time as the particles move.

By definition, different streamlines in a flow do not intersect at the same instant, because a fluid particle cannot have two different velocities at the same point. Similarly, streaklines cannot intersect with themselves or other streaklines, because two particles cannot be present at the same location at the same instant of time, unless the point of origin of one of the streaklines also belongs to the streakline of the other point of origin. However, pathlines are allowed to intersect with themselves or other pathlines (except the starting and end points of the different pathlines, which need to be distinct).

Streamlines and timelines provide a snapshot of some flowfield characteristics, whereas streaklines and pathlines depend on the full time-history of the flow. However, often sequences of timelines (and streaklines) at different instants—being presented either

in a single image or with a video stream—may be used to provide insight in the flow and its history.

Boundary Layer

In physics and fluid mechanics, a boundary layer is the layer of fluid in the immediate vicinity of a bounding surface where the effects of viscosity are significant.

Laminar boundary layers can be loosely classified according to their structure and the circumstances under which they are created. The thin shear layer which develops on an oscillating body is an example of a Stokes boundary layer, while the Blasius boundary layer refers to the well-known similarity solution near an attached flat plate held in an oncoming unidirectional flow. When a fluid rotates and viscous forces are balanced by the Coriolis effect (rather than convective inertia), an Ekman layer forms. In the theory of heat transfer, a thermal boundary layer occurs. A surface can have multiple types of boundary layer simultaneously.

The viscous nature of airflow reduces the local velocities on a surface and is responsible for skin friction. The layer of air over the wing's surface that is slowed down or stopped by viscosity is the boundary layer. There are two different types of boundary layer flow: laminar and turbulent.

(1) Laminar Boundary Layer Flow

The laminar boundary is a very smooth flow, while the turbulent boundary layer contains swirls or "eddies." The laminar flow creates less skin friction drag than the turbulent flow, but is less stable. Boundary layer flow over a wing surface begins as a smooth laminar flow. As the flow continues from the leading edge, the laminar boundary layer increases in thickness.

(2) Turbulent Boundary Layer Flow

At some distance back from the leading edge, the smooth laminar flow breaks down and transitions to a turbulent flow. From a drag standpoint, it is advisable to have the transition from laminar to turbulent flow as far aft on the wing as possible, or have a large amount of the wing surface within the laminar portion of the boundary layer. The low energy laminar flow, however, tends to break down more suddenly than the turbulent layer.

Reynolds Number

In fluid mechanics, the Reynolds number (Re) is a dimensionless quantity that is used to help predict similar flow patterns in different fluid flow situations.

The Reynolds number can be defined for several different situations where a fluid is in relative motion to a surface. These definitions generally include the fluid properties of density and viscosity, plus a velocity and a characteristic length or characteristic dimension. This dimension is a matter of convention – for example radius and diameter are equally valid to describe spheres or circles, but one is chosen by convention. For aircraft or ships, the length or width can be used. For flow in a pipe or a sphere moving in a fluid, the internal diameter is generally used today. Other shapes such as rectangular pipes or non-spherical objects have an equivalent diameter defined. For fluids of variable density such as compressible gases or fluids of variable viscosity such as non-Newtonian fluids, special rules apply. The velocity may also be a matter of convention in some circumstances, notably stirred vessels. The Reynolds number is defined in equation 2.5 for each case, where:

$$\text{Re} = \frac{\text{inertial force}}{\text{viscous force}} = \frac{\rho v L}{\mu} = \frac{v L}{\nu} \quad (2.5)$$

v is the maximum velocity of the object relative to the fluid (SI units: m/s)

L is a characteristic linear dimension, (travelled length of the fluid; hydraulic diameter when dealing with river systems) (m)

μ is the dynamic viscosity of the fluid (Pa·s or N·s/m² or kg/(m·s))

ν is the kinematic viscosity ($\nu = \mu/\rho$) (m²/s)

ρ is the density of the fluid (kg/m³). Note that multiplying the Reynolds number by

$L\nu/L\nu$ yields $\frac{\rho v^2 L^2}{\mu \nu L}$, which is the ratio of the inertial forces to the viscous force.

Boundary layer is taken as the distance between the surface of object and the outside fluid current where the velocity is increasing along the direction of the normal line from zero to same as free flow velocity of outside, U (specifically speaking, it equals to 0.990 or 0.995 U).

The thickness of boundary layer has relationship with the Reynolds number of the flow, the conditions of the free flow, surface roughness of the object, shape of the object and the extended field. From the head (leading edge) of the flow-passed object, the thickness of the boundary layer thickens and gradually increases in the direction of the flow from zero. When the Reynolds number of an atmosphere flow, $Re_x=10^6$, 1m from the leading edge, the thickness of the boundary layer in the upper flow on the plate is 3.5mm.

On the smooth plate, the thickness of boundary layer in laminar flow is shown as follows:

$$\delta(x) \propto \sqrt{\nu x / U} \quad (2.6)$$

or

$$\delta(x) \propto x / \sqrt{\text{Re}_x} \quad (2.7)$$

$\text{Re}_x = Ux/\nu$, where ν is the viscosity of the fluid. When it is written in equation, constant value will differ according to the velocity percentage of selected boundary layer (such as, 0.90, 0.99 or 0.995U); commonly, it is in the range of 3.46 to 5.64.

On the smooth plate, the thickness of the boundary layer in upper turbulent flow is as follows:

$$\delta(x) \propto x / \sqrt[5]{\text{Re}_x} \quad (2.8)$$

Its ratio constant is approximately 0.37. It can be seen that there exists randomness while measuring the boundary layer so that it can give accurate values. Therefore, in this study, the boundary layer is discussed briefly based on the theory of fluid mechanics for describing the influence of different immersed positions of silicon wafers to be etched.

CHAPTER 3

EXPERIMENTAL

3.1 Research Purpose

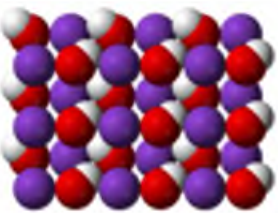
In this research study, the goal is to etch silicon wafers using KOH solution with simplified devices, compare the differences in surface morphology of samples to determine the better etching conditions and finally obtain uniformly surface-etched silicon wafers, which can be used in the fabrication of solar cells. The objective is to make the etching process to be controllable and predictable, including surface morphology and etch rates.

3.2 Substrate

P-type front-surface polished and backside masked Shin-Etsu (SEH AMERICA, INC.) silicon wafers with (1 0 0) orientation, 14.8-17.2 μ m thickness and 14-21 Ω -cm resistivity were used for studying the anisotropic etching experiments.

The etchant in etching solutions were prepared from analytical grade potassium hydroxide pellets, PX1480-1, GR ACS by EMD Millipore Corporation, an affiliate of Merck KGaA, Darmstadt, Germany. The properties of KOH are given in Table 3.2.

Table 3.2 Basic properties of Potassium hydroxide (KOH)

Molecular structure	Molar mass	Density	Boiling point	Melting point
	56.1056 g/mol	2.12 g/cm ³	2,421°F (1,327°C)	762.8°F (406°C)

Source: Wikipedia, https://en.wikipedia.org/wiki/Potassium_hydroxide.

The distilled water, used for the experiments, was supplied by the Chemistry Department at NJIT.

3.3 Apparatus

The etching experiments used a magnetic heating agitator, a thermometer, a magnetic stirrer, two ring stands (one for fastening the thermometer, another for fastening the silicon wafer), many clips for fastening related instruments, a beaker for reaction vessel and any other fundamental laboratory equipment for preparing solution and surface cleaning, such as beakers, volumetric flasks, electronic balance, liquid dropper, stirrer glass rod, medicine spoon, weighing papers and so on.

The experimental system was setup in a chemical hood to ensure that the system is on a horizontal platform. During the etching process, the hood is operated in air bleeding mode.

The beaker for reaction was located at the center of the heating agitator so that the magnetic stirrer would not hit the wall of the beaker during stirring.

The immersed position of thermometer is away from the bottom of the beaker with the distance of one fourth the height of the beaker. In this way, it could measure the temperature of etching solution as accurate as possible because the large fluctuations in temperature may have negative influence on the etching results. Besides, the thermometer cannot also be in contact with the wall of the beaker and the stirrer.

The stirring speed was controlled in low level to avoid forming vigorous eddy currents in the center of the solution.

With the aid of ring stand and clips, the immersed position and direction of silicon

wafer could be adjusted.

The established experimental apparatus is shown below, (the two ring stand is omitted in this diagram)

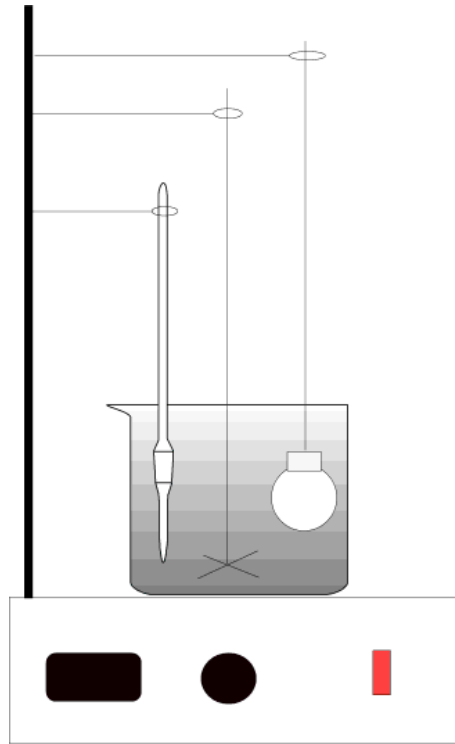


Figure 3.3 Simplified schematic diagram of experimental apparatus.

An aluminum foil was used to cover the top of the beaker in order to reduce the loss of water by evaporation, which would change the etchant concentration in the solution with increasing reaction time.

3.4 Procedure

P-type front side polished silicon wafers with (100) orientation, were used for investigating the anisotropic etching experiments. After the standard surface cleaning process using acetone and methanol, wafers were dried in room temperature and pressure. After the moisture was removed, KOH etching was carried out at various concentrations (1mol/L

and 2mol/L) and different temperatures (50°C and 70°C) with different etching time (30 minutes, 60 minutes). Additionally, in order to determine the best immersed wafer position in the experiments for etching uniformity, vertical, tangent and parallel positions were examined with the etching condition of 1mol/L KOH solution at 70°C for 60 minutes. After etching process, the samples were rinsed carefully by distilled water and dried at room temperature and pressure.

It is worth noting that the procedure did not involve HF (Hydrofluoric acid) pre-cleaning during surface cleaning process.

All the experiments were carried out in a closed glass vessel with a constant temperature bath. A magnetic stirrer rotating at a speed of 200 rpm was used continuously during etching to facilitate uniform etching.

3.5 Characterization Methods

After etching, wafer surfaces were examined by scanning electron microscopy (SEM) to investigate the surface morphology. Profilometer was used to determine the change in morphology in etched silicon wafer. The surface reflectivity was measured using a Graseby Infrared Cavity Black-body Reference.

The characterization methods used in this study included the following: (i) Raman spectroscopy to analyze vibration of molecules for identifying the species in silicon wafers; (ii) Profilometer to estimate the change in thickness of silicon wafers during the etching process; (iii) SEM to compare the surface morphology; and (iii) Infrared black-body reference to measure reflectivity.

CHAPTER 4

RESULTS AND DISCUSSION

4.1 Comparison of Silicon Etch Rates in Different Conditions of KOH Solutions

In order to analyze the etching characteristics of KOH and to obtain a better control of the etch process for a uniformly rough surface, the silicon etch rates at different concentrations and temperatures of KOH solutions have been investigated. The Raman spectra of the etched samples are shown in Fig 4.1.1.

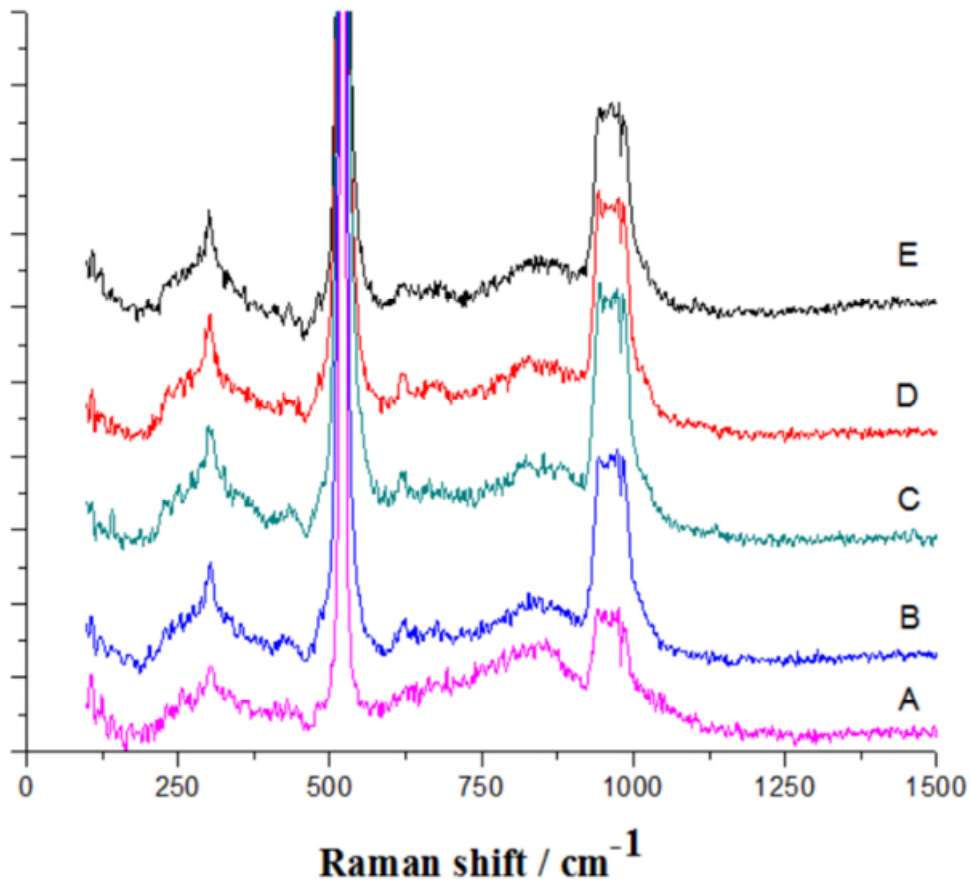
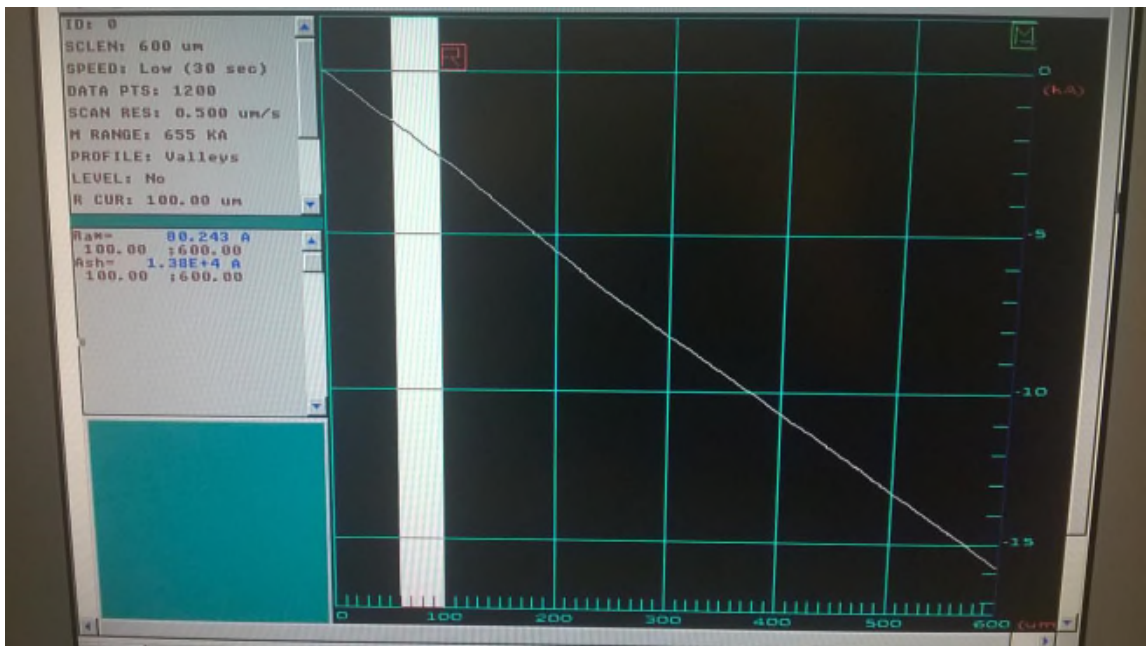


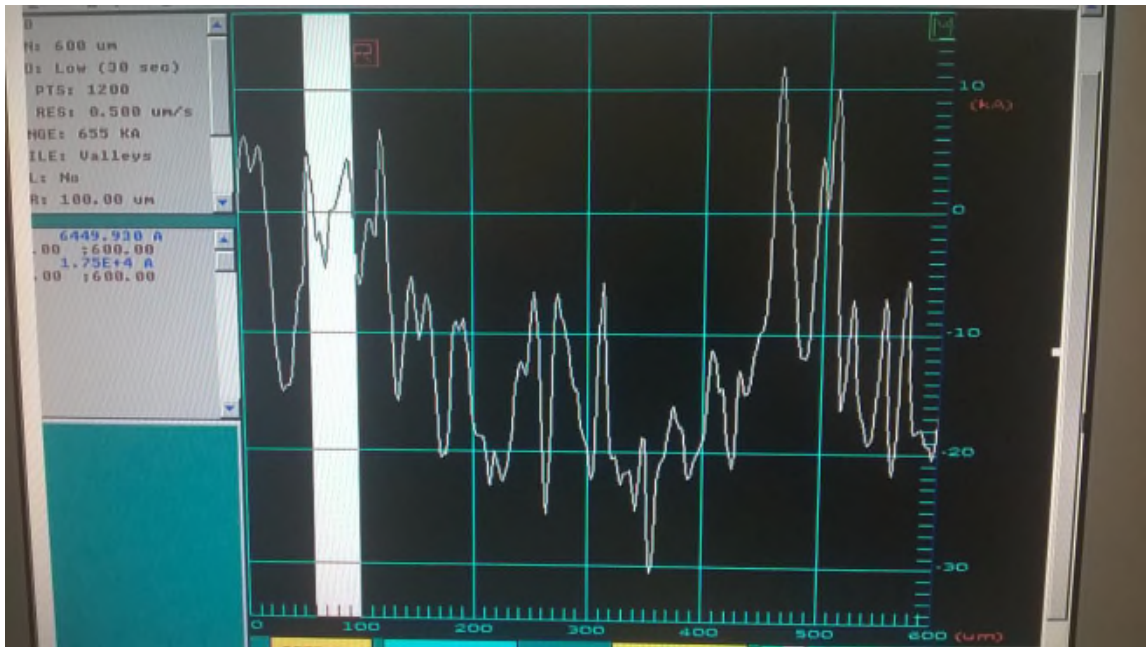
Figure 4.1.1 Raman spectra of samples. A. Substrate silicon wafer without any treatment; B. Sample etched in 1mol/L, 70°C, 1h; C. Sample etched in 1mol/L, 70°C, 0.5h; D. Sample etched in 1mol/L, 50°C, 1h; E. Sample etched in 2mol/L, 70°C, 1h.

From Figure 4.1.1, it can be seen that there is a strong peak at $\sim 522\text{cm}^{-1}$ indicating the vibration modes of silicon atoms. Other weak peaks appear at $\sim 300\text{cm}^{-1}$ and $\sim 900\text{cm}^{-1}$ (Integrated Chemical Database, <http://rruff.info/Silicon>). Although there are no accurate references to identify these two weak peaks, it can hardly be ruled out that the possibility of these two weak peaks can be attributed to the dopants or impurities (the substrate silicon wafer is p-type which is mentioned above) in the silicon wafer.

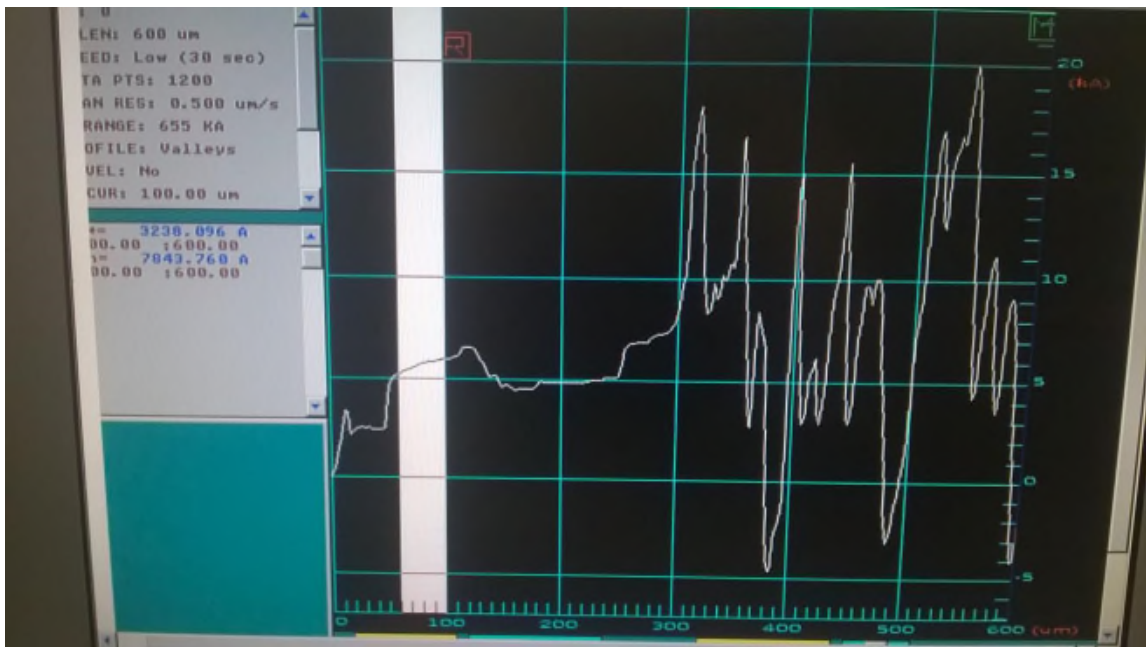
In order to investigate the surface profiles of the etched wafers, samples after etching under various etching conditions were measured by a profilometer. Fig. 4.1.2 shows the results of the Si (100) plane at different KOH concentrations, temperatures and etching times. The results were obtained using Dektak3 profilometer. During the measurements, there was mechanical failure due to the inability to adjust the level of the profilometer along the horizontal. Moreover, the profilometer did not provide any option to collect the output data. Therefore, the screenshots of these profilometer data are presented in Figure 4.1.2.



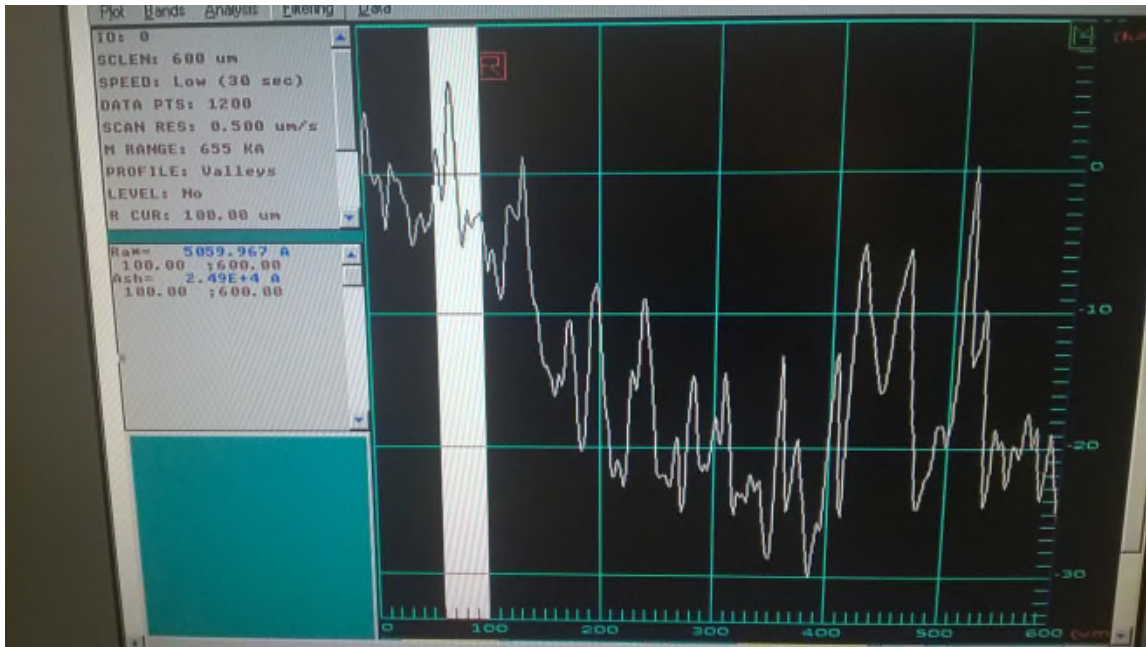
(a)



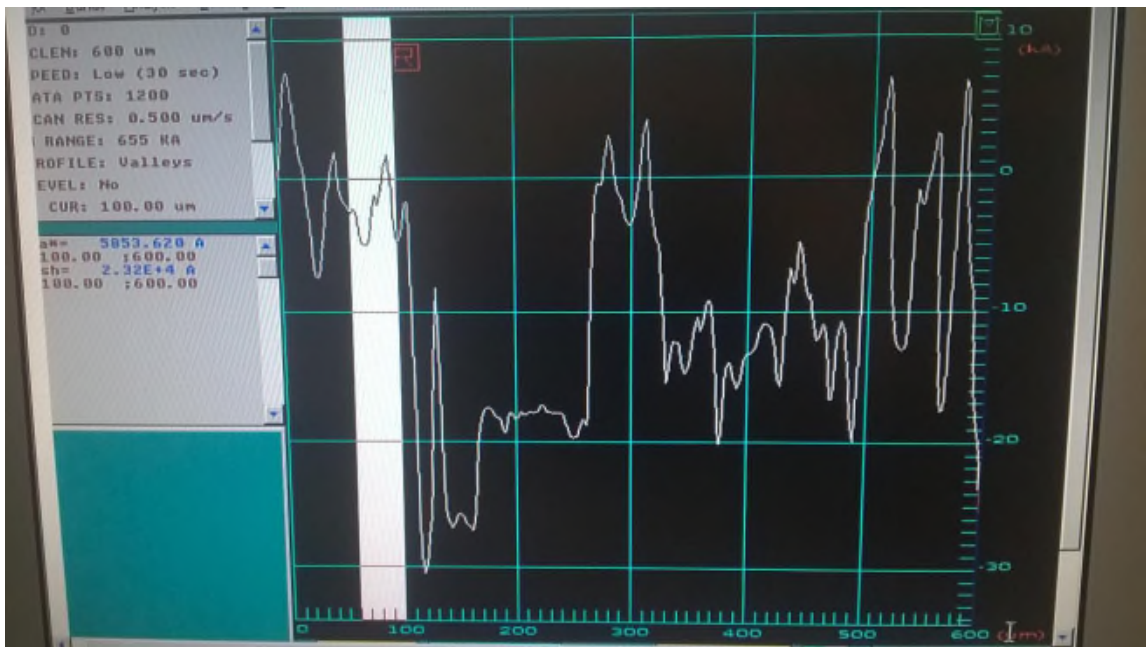
(b)



(c)



(d)



(e)

Figure 4.1.2 Screenshots of profilometer spectrograms of samples. (a) Substrate silicon wafer without any treatment; (b) Sample etched in 1mol/L, 70°C, 1h; (c) Sample etched in 1mol/L, 70°C, 0.5h; (d) Sample etched in 1mol/L, 50°C, 1h; (e) Sample etched in 2mol/L, 70°C, 1h.

Since there are no masks on the surface of the silicon wafers, in this study, the existence of undercut is not considered. Also, lack of patterning means that the etched

thickness cannot be measured as there are no surfaces to be taken as the basis for such measurements. However, the surface distribution of peaks and forms of pyramidal or hillock structures can be seen on the surface of the etched silicon wafer in the spectrograms.

Although, there is a right slant within a few micrometers in Fig 4.1.2(a), it is clear that the silicon wafer, without any etching treatment, has a straight and smooth surface. This suggests that within random selected linearity region of $600\mu\text{m}$, the profilometer can show the trends in distribution of pyramidal and hillock structures and their thickness. According to this, Fig 4.1.2(b) shows that, in the $600\mu\text{m}$ region, the absolute values of peaks tend to be similar in where there are no extreme high or wide peaks, which means that the surface roughness is uniform and the etch rate is similar for the peak structures during the etch process; Fig 4.1.2(c) shows that, ignoring interference between $0\text{-}300\mu\text{m}$ may be caused by any mechanical errors or impurities on the surface of the silicon wafer. In the region of $300\text{-}600\mu\text{m}$, there were several different sizes and scales of peaks, which means that the etching reaction did not sufficiently and uniformly take place and some areas with low potential barriers on the surface tended to react faster than other areas within short etching time. Fig 4.1.2(d) shows that there are different sizes of peaks, which indicates that uniform pyramidal or hillock structures did not form on the surface because of low temperature. Fig 4.1.2(e) shows that there appears a flat area zone and short peaks, which indicates that, with increase in concentration of the etchant, the etch rates increase simultaneously and lead to shrinkage in pyramidal structure and tend to disappear where they will form flat areas in the end.

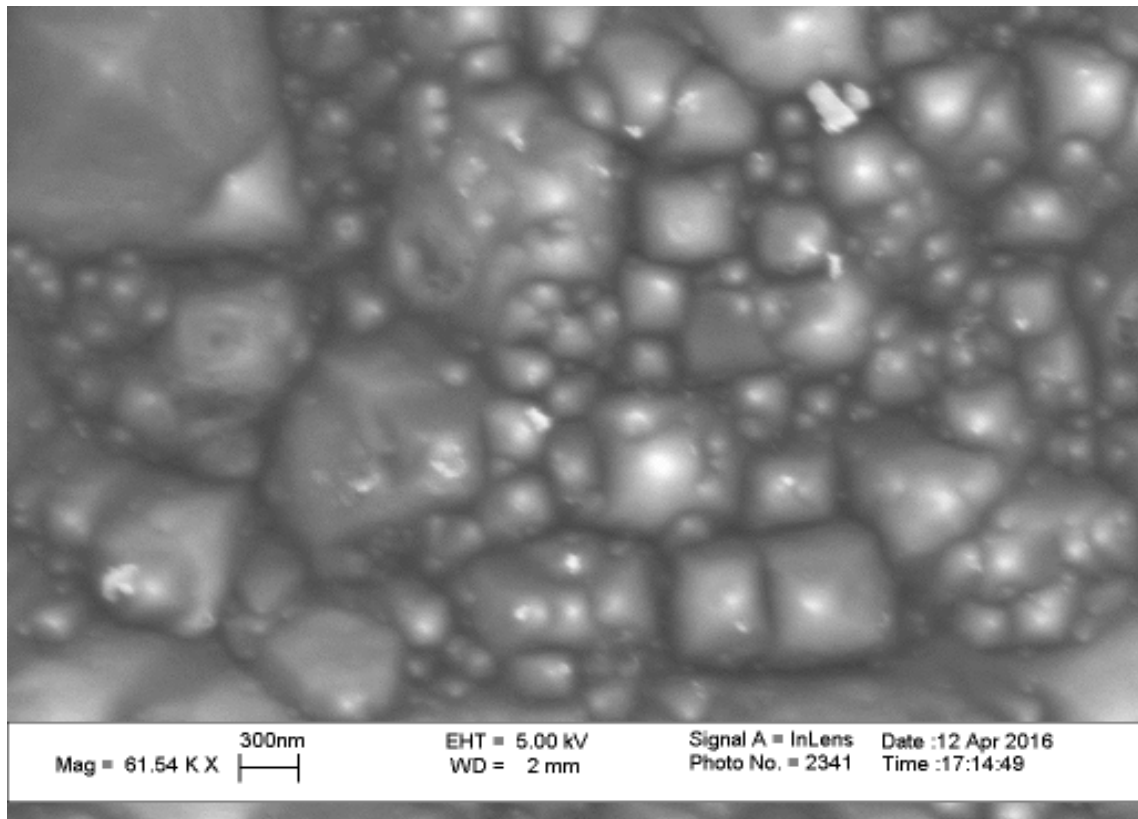
Above all, Fig 4.1.2 shows that the (100) plane etch rates increase with increase in temperature, Increase in solution concentration can also increase the reaction rate. The increase in both temperature and solution concentration may have adverse effects on the formation of uniform pyramidal or hillock structures.

According to the model of etching process, investigated by Seidel et al. [17], the etch rate of silicon depends on the amount of hydroxide ions and free water concentration ($R \approx [\text{H}_2\text{O}]^a \times [\text{OH}^-]^b$) in etching solution. With the increase in concentration of solution, the content of hydroxide ions increases. However, because the ionized ions (K^+ , OH^-), resulting from the dissociation of resolved KOH molecule, undergo hydration in the solution, they consume quite an essential portion of water. Therefore, the combined effect of the increased hydroxide ions and the decreased free water concentration leads to slight decrease in the (1 0 0) plane etch rate with KOH concentrations.

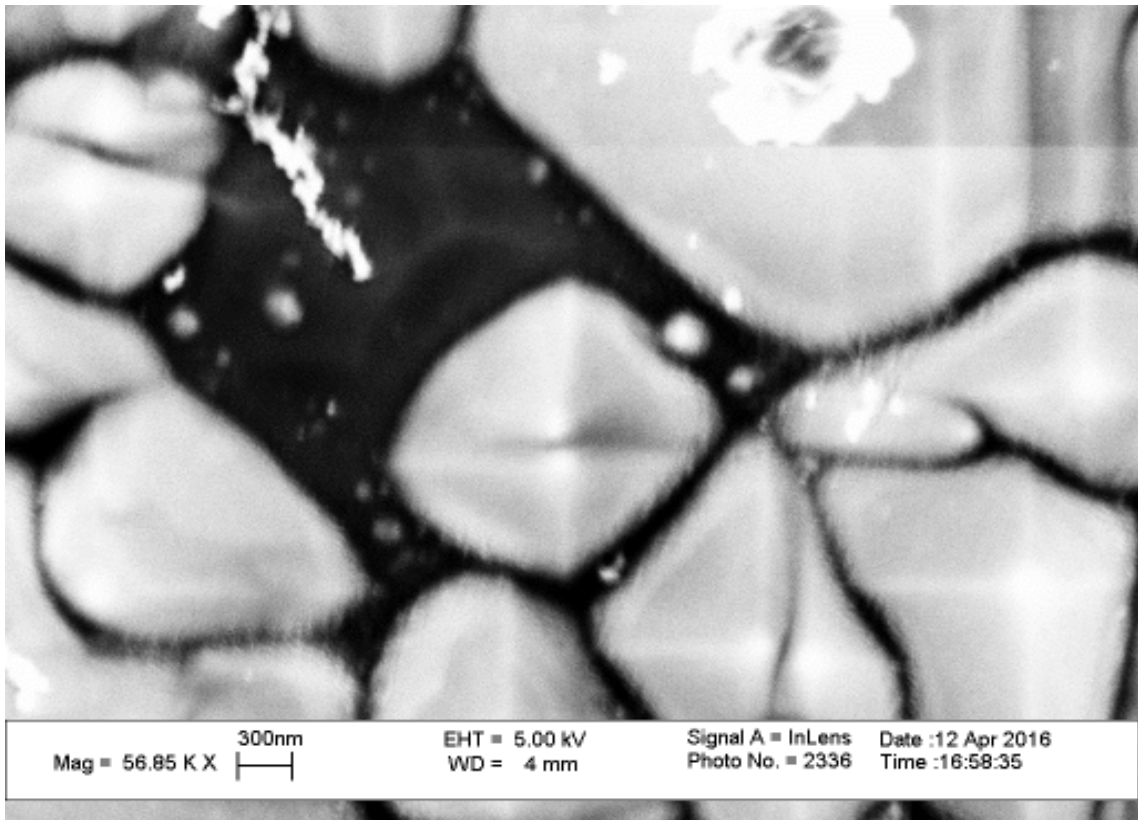
The (1 1 1)/(1 0 0) etch rate ratio can be calculated by dividing etched depth of the (1 1 1) plane by the etched depth of the (1 0 0) plane. The etched depth of the (1 1 1) plane can be calculated by multiplying the overhanging oxide depth by $\sin 54.74^\circ$ (see in Equation (2)) to analyze the influence of differences in etching conditions. However, with limited data and measurement methods, in this study, this part of the analysis was not realized.

4.2 Comparison of Surface Morphologies Etched by Different Conditions of KOH Solutions and Different Immersed Positions

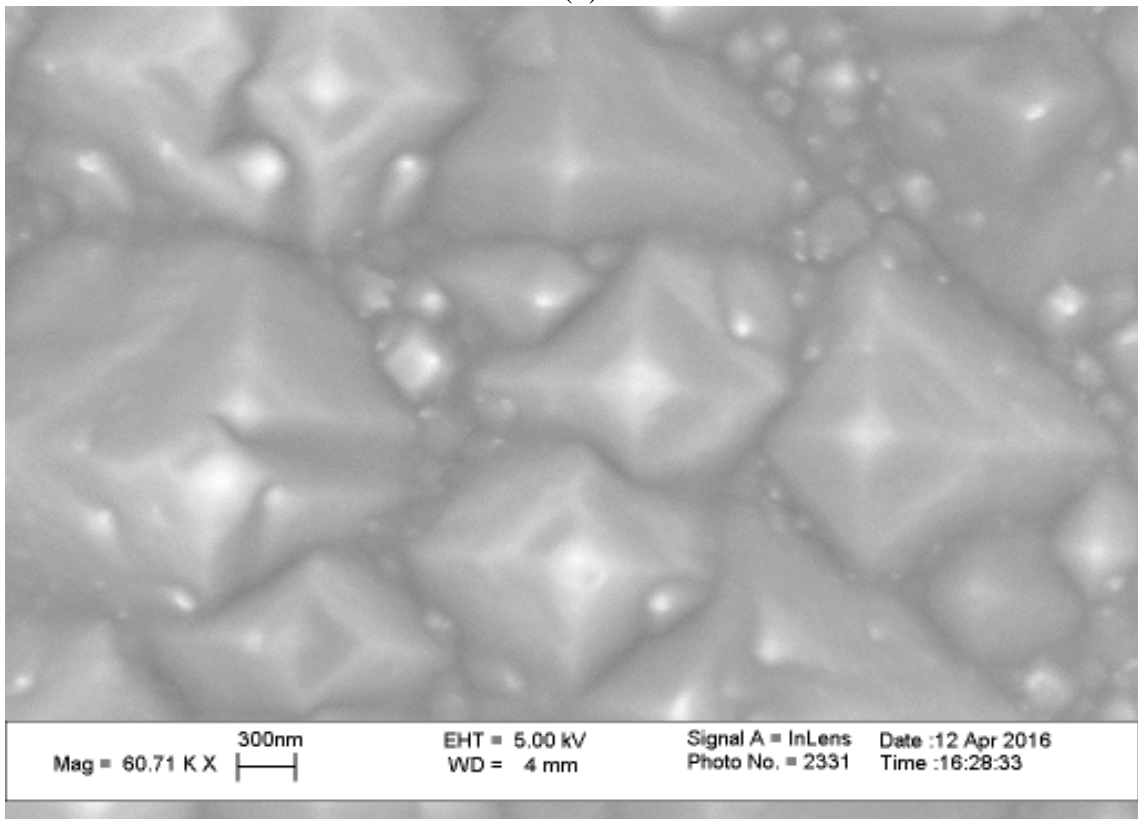
In KOH solution, because of large amount of OH^- in solution, the etch rate will change depending on different etching conditions. Etching produces a few tiny bubbles of H_2 , which will overflow resulting in a decrease in the etching reaction. The SEM images show the surface morphology of silicon surfaces etched under different etching conditions (time, temperature and concentration). By comparing surface morphologies, the better etching conditions that lead to better surface uniformity can be identified.



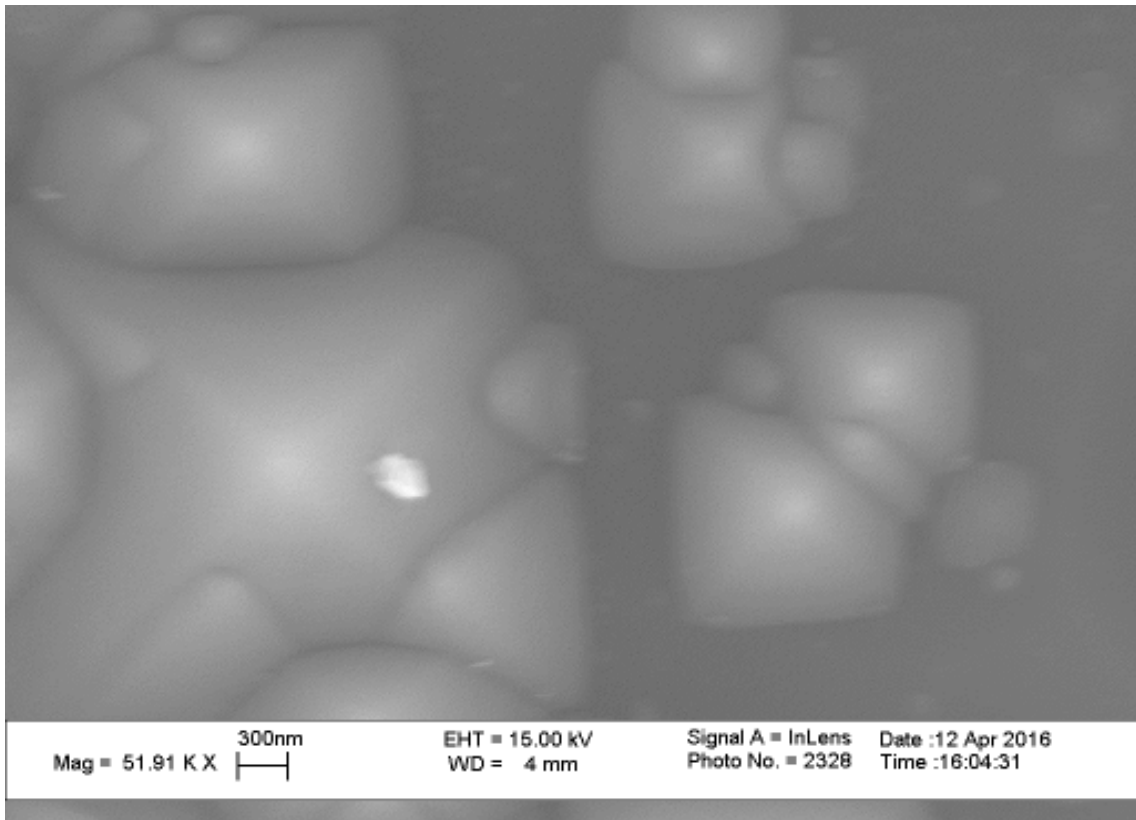
(a)



(b)



(c)



(d)

Figure 4.2.1 SEM images of etched Si surface morphology showing pyramidal and hillock structures. (a) Sample etched in 1mol/L, 70°C, 1h; (b) Sample etched in 1mol/L, 70°C, 0.5h; (c) Sample etched in 1mol/L, 50°C, 1h; (d) Sample etched in 2mol/L, 70°C, 1h.

Generally, the surfaces of all samples look like suede. With lower EHT, the image is more detailed and difference in WD means different heights of sample appear. The formation of pyramids and hills on silicon surface, after etching, can affect the ability to trap light in the final solar cell structure. In order to enhance light trapping, the silicon surface should be rough enough for incident light to go through multiple reflections repeatedly so that, in each time of reflection, the incident light will lose intensity through refraction and absorption. In other words, in order to enhance light trapping, there is a need to form uniform rough surface with optimized roughness characteristics, namely pyramidal and hillock structures, on the silicon surface after etching. Moreover, optimized roughness

is also a reference standard to evaluate etching results as a preliminary step. In the following part, comparisons of different etching conditions will be discussed.

Difference in Etching Time

Comparison studies of the SEM images of sample (a) and (b), which were etched for different etching time, is discussed in this section. In sample (b), with 30 minutes of etching time, it can be seen that the silicon surface produces generally large hills with different sizes. The diameters of big hills can reach $10\mu\text{m}$ or more (refer to supplementary diagram Fig 6.2(a)) because the etching reaction is not uniform and is in progress within the short etching time. At this point of reaction, there exist a large number of defects, with lower potential barrier and higher chemical activity on the surface of the silicon wafer, which can be etched easily by alkali ions than other areas. When etching time is increased to 60 minutes in sample (a), the etch hills become smaller and more regular in size, though there still exist a few big hills; the diameter decreases to approximately 300nm , some part of smaller hills tend to disappear because of the collapse in etch hillock structure. The hills are arranged closely and embody a uniform roughness. As a result, it is concluded that samples etched in 1mol/L , 70°C , 1h have better surface morphology.

Difference in Etching Temperature

In this section, a comparison of the SEM images of sample (a) and (c), which were etched at different etching temperatures, is presented. In sample (c) with 50°C of etching temperature, it can be seen that the silicon surface produces uneven size of hills. The diameter of bigger hills can reach $1\mu\text{m}$ or more and they are not closely arranged. There was no appearance of regular and ordered pyramidal structure. When etching temperature is increased to 70°C in sample (a), the size of etch hills become more uniform. The

increased temperature will quicken the etch rate. It can be inferred that, in going to higher temperatures, the etch hills will finally disappear. It is thus clear that temperature has significant influence on forming pyramidal structures. It is the optimal condition for obtaining the best etching results and beyond it, the etching results will turn worse because of the disappearance of etch hills.

Difference in Etchant Concentration

A comparison of the SEM images of sample (a) and (d), which were etched with different concentrations of etchant (KOH) is presented in this study. In sample (d), with 2mol/L of KOH, it can be seen that the silicon surface produces smaller and dispersive etch hills and black underside, which means the etch hills completely disappear in those areas. Although the resolution is different, in supplementary diagram Fig 6.2(b), many stages of such disappearance of etching hills can be observed. In the early stages of disappearance, the hills are attacked in a way to be expected considering its shape, namely the top disappears, followed by the protruding (110) orientation. This etching proceeds quickly and the new generated surface, which is nearby, is of (100) orientation. The early stage continues until the side faces of the hillock are completely etched away. On the contrary, in sample (a) with 1mol/L of KOH, the bottom areas cannot be seen. It is thus clear that the etchant concentration also has significant influence on etching results and should be controlled.

Geometrically speaking, experimental evidence shows that the concentration and temperature of the etchant are the main parameters that influence the size and number of the pyramidal structures and etch hills; however, these pyramidal etch hillocks are unstable

and sensitive to change in etching solution. It is necessary to balance the parameters discussed above to reach ideal etching results.

Sample Position

As the research progressed, the etching results showed that the specific parallel position (with respect to the etchant) can lead to much higher quality of smooth and uniform (100) crystal faces and uncontaminated surfaces than that of other positions such as change in angles (Table 4.2). Hence, for the study of the effect caused by different immersed position of silicon wafer in etching solution, a set of samples were etched in 1mol/L KOH solution at 70°C for 60minutes for three different immersed positions: parallel, tangent and vertical.

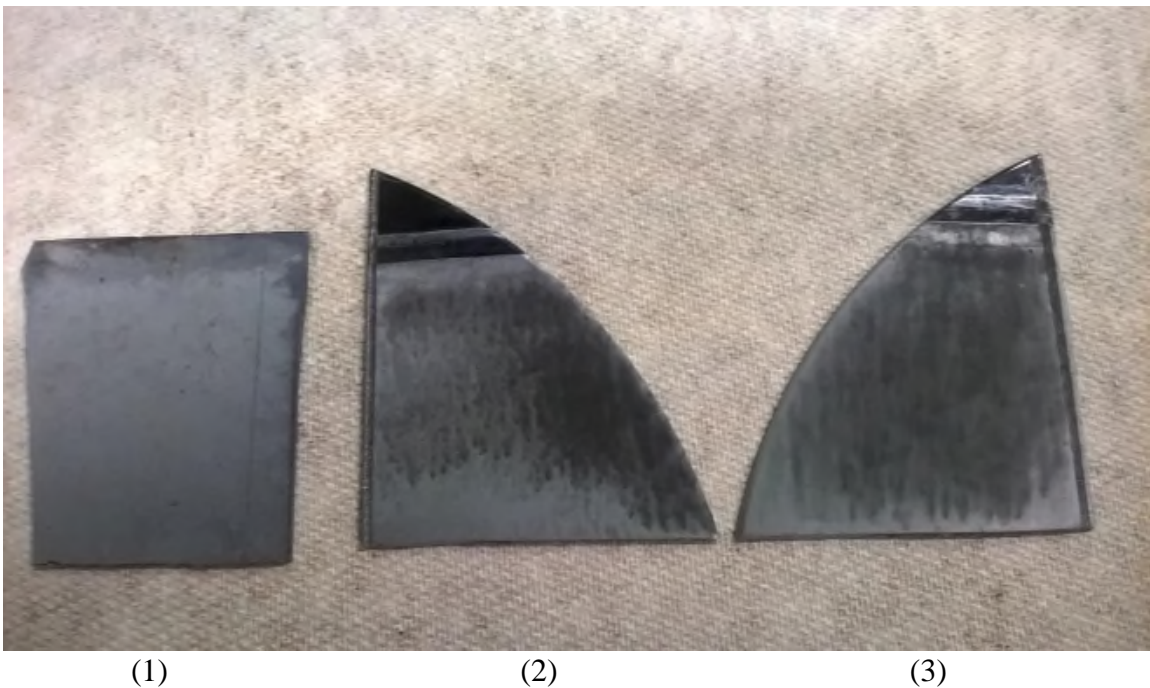


Figure 4.2.2 Photograph of etched samples immersed in different positions. (1)Sample etched in parallel position; (2)Sample etched in tangent position; (3)Sample etched in vertical position. All the samples were etched in 1mol/L KOH solution at 70 °C for 60 minutes.

Fig 4.2.2 shows the etched surfaces of silicon wafers etched in three different immersed positions. From the visible effects, it can be observed that the surface of vertical position silicon wafer seems to be less uniformly etched and even “violently” damaged in

certain areas. The surface of tangent position silicon wafer seems to be better than that of the vertical position. There is still considerable non-uniformity on the etched surface. By contrast, the surface of parallel immersed silicon wafer appears to be more uniformly etched than the other two samples.

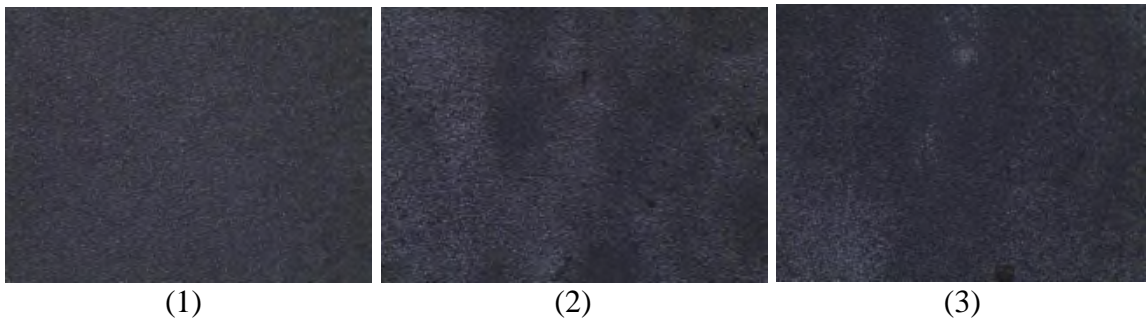
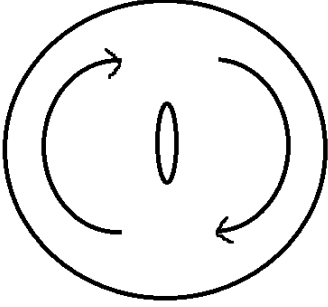
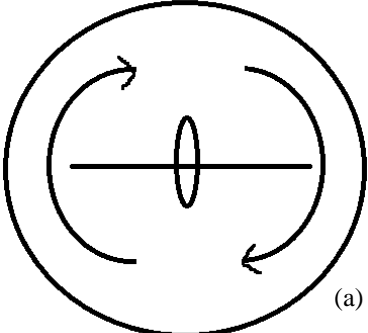
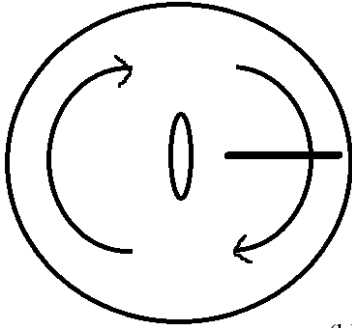
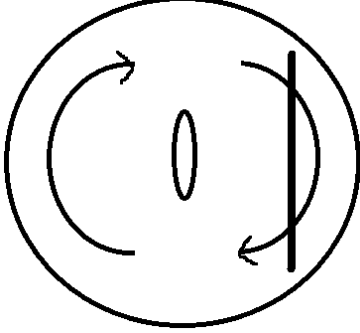
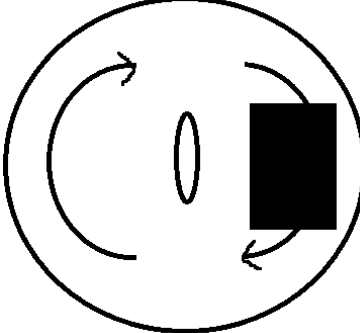
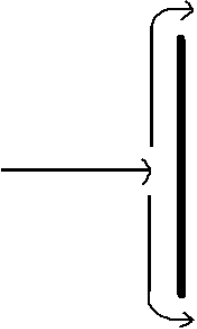
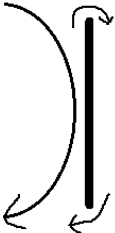



Figure 4.2.3 Optical micrograph of etched sample immersed in different positions. (1) Sample etched in parallel position; (2) Sample etched in tangent position; (3) Sample etched in vertical position. All the samples were etched in 1mol/L KOH solution at 70 °C for 60 minutes.

Fig 4.2.3 shows the optical micrographs of etched surface of silicon wafers etched in three different immersed positions. The sample etched in parallel position was much more uniform than other positions.

The surface morphologies of silicon wafers with (100) orientation, etched in vertical, tangent and parallel, have been analyzed using profilometer as shown in the supplementary diagram Fig 6.1. From Fig 6.1(a), it can be found that the (100) surface is etched unsatisfactorily in tangent position. Although there were hills formed on the surface, altitudes of etch hills and distribution of roughness can hardly meet the requirement of enhanced light trapping. From Fig 6(b), it can be seen that the (1 0 0) surface is etched non-uniformly. The extreme high hills mean that the etch rates were not uniform on the surface which lead to such areas with low potential barriers that are etched quickly and other areas that are etched slowly.

Table 4.2 Top View of Immersed Positions of silicon wafer

			
Immersed positions of silicon wafer	Vertical	Tangent	Parallel
	 (a)  (b)		
Streamlines in flow field			

With limited knowledge and data, this research attempts to give explanations that are in accord with the theory of fluid mechanics. Table 4.2 shows three different kinds of immersed position. After surface morphology analysis, it can be inferred that there may exist some factors other than chemical reaction, such as physical effects or mechanics of fluid flow, the relative contact position between immersed wafer and flow patterns of the stirred etching solution, that have potential influence on etching results. On the basis of the theory of fluid mechanics, a boundary layer forms in the interface between fluid and surface of silicon wafer during etching reaction when the flow velocity is in a certain range of values. Within the boundary layer, the flow velocity begins to increase gradually from zero at the surface of the silicon wafer to the velocity of outside flow in etching solution. The diffusion of reactants, needed for the etching reaction, will take place in this boundary layer. The thickness of boundary layer is inversely proportional to the flow velocity which is determined by the Reynolds number (Re) illustrated in the literature review. Eliminating other interference factors, for example the size of the beaker, shape of silicon wafer, even size of clips and so on, and only focusing on the flow velocity, boundary layer thickness and etch rate (etching reaction rate), after taking flow field and streamlines (the trail of fluid flowing) into consideration, the vertical position has the minimum velocity across the surface among three positions because of the minimum momentum of fluid flow. With lower flow velocities, it has more stagnant reactants and products between silicon wafer and etching solution. This causes unequal etch rates across the surface of the silicon wafer which could lead to lower and less uniform etching rates and poorer surface morphologies. The analytic order of flow velocity among three positions is: parallel > tangent > vertical. With the analysis of microscope images, it is clear that parallel position has better surface

performance than others, which indicate that it has led to more complete and uniform reaction between silicon wafer and etching solution when flow velocity is high across the surface. As a result, interestingly, the performance of surface morphology (the uniformity and smoothness) is: parallel > tangent > vertical. Thus, higher flow velocities lead to more complete etching reactions.

However, at the present stage, these discussions still remain a hypothesis. In order to explain this phenomenon, more data, with more sensitive measurements, is needed.

4.3 Surface Reflectivity Analysis

Surface reflectivity is a critical parameter for the performance of solar cells. In general, the UV-VIS(-NIR) spectroscopy will be the best choice for measuring the reflectivity because it can provide reflectivity data of samples for a wide range of wavelengths. However, in this study, the samples were measured by black-body infrared radiation system instead of UV-VIS spectroscopy. Table 4.3 summarizes the various IR images of samples after etching in different conditions. The polished front-side of the silicon wafers were etched and, by contrast, the masked backsides of each sample of the silicon wafer were taken as the reference images for comparison.

An infrared imager, manufactured by FLIR[®] Systems, Inc., was used as the infrared detector for measuring the response from the sample in the infrared range of wavelengths.

The thermal effects of the incident IR radiation can be followed by many temperature dependent phenomena. Bolometers and microbolometers respond to changes in resistance. Thermocouples and thermopiles use the thermoelectric effect. Golay cells follow thermal expansion. In IR spectrometers, the pyroelectric detectors are the most widespread. The response time and sensitivity of photonic detectors can be much higher, but usually these have to be cooled to cut thermal noise. The materials in these are semiconductors with narrow band gaps. Incident IR photons can cause electronic excitations. In photoconductive detectors, the resistivity of the detector element is monitored. Photovoltaic detectors contain a p-n junction on which photoelectric current appears upon illumination.

Although the measured wavelength was limited in infrared, it can still indicate the strength and intensity of the sample surface reflectivity.

Table 4.3 Reflectivities Measured with Black-Body Infrared Radiation System

	Front side (etched)	Backside(masked)
(a)	<p>max 36.3°C ϵ 0.70 30.5 26.5 FLIR</p>	<p>max 69.1°C ϵ 0.70 30.5 26.5 FLIR</p>
(b)	<p>max 38.2°C ϵ 0.70 30.8 26.7 FLIR</p>	<p>max 68.1°C ϵ 0.70 31.2 27.2 FLIR</p>
(c)	<p>max 53.9°C ϵ 0.70 31.0 27.0 FLIR</p>	<p>max 128°C ϵ 0.70 30.8 26.8 FLIR</p>
(d)	<p>max 32.5°C ϵ 0.70 31.1 27.0 FLIR</p>	<p>max 71.0°C ϵ 0.70 30.7 26.6 FLIR</p>

(a) Sample etched in 1mol/L, 70°C, 1h; (b) Sample etched in 1mol/L, 70°C, 0.5h;
(c) Sample etched in 1mol/L, 50°C, 1h; (d) Sample etched in 2mol/L, 70°C, 1h.

The temperature values in these images, captured by the infrared detector, not only reflect the real temperature of the surfaces of the samples but also suggest the intensity of reflectivity at this point. However, during the measurement, in order to direct the focus of the camera, the relative positions of the black-body source, sample and FLIR camera were changed, which led to inaccuracy in measurement and unreliability of the measured data. Yet, in basic analysis of reflectivity, although there exists fluctuation in temperature, it can be seen that the sample etched in 2mol/L KOH solution at 70°C for 1hour has the lowest temperature which indicates that this sample has the lowest reflectivity among all the samples. The etching condition corresponding to this sample might be interpreted as the optimal condition.

With more reliable and accurate data, the optimal condition for etching can be determined and this will be the further work for the future.

CHAPTER 5

CONCLUSION

In this work, comparative etching experiments of using KOH solution on silicon wafers have been carried out for different etchant concentrations (1mol and 2mol) and different temperatures (50°C and 70°C) with different etching time (30minutes and 60minutes) to prepare uniformly rough surfaces. Furthermore, in order to investigate the best immersed position that maybe have potential influence on etching results during the etching experiments, positions of vertical, tangent and parallel were examined and the samples were respectively etched in 1mol/L KOH solution at 70°C for 60 minutes. It has been found that the change in temperature and etchant concentration have significant influence on etching results. More importantly, the surface morphology analysis shows that increased temperature can contribute to form more arranged pyramidal and hillock structures. Additionally, parallel immersed position has uniform etch rate than any other immersed position after preliminary analysis according to the fluid mechanics and suggests a hypothesis of relation between etch rate, fluid velocity and boundary layer. Finally, the preliminary reflectivity analysis of the samples shows that minimum reflectivity is observed with etching condition of 2mol/L, 70°C for 60 minutes, which can be considered as reaching the ideal etching condition in the present study. In summary, without common etching conditions, the immersed position also has attractive influence in forming uniformly rough surface, which means that the etching process needs to manage all conditions well so that light entrapment will be enhanced.

FUTURE WORK

It has to be recognized that there is still extensive work that needs to be done on the subject in the future. The samples need to be prepared, measured and analyzed with more controlled and sensitive measurement methods.

Firstly, more experiments, with varied etching conditions, must be performed in order to determine the optimal etching condition.

Secondly, the relationship between the etch rate uniformity and fluid velocity must be established with sufficient experimental data.

Thirdly, complete analysis of reflectivity, for a wide range of wavelengths, is required to be able to quantify light trapping.

REFERENCES

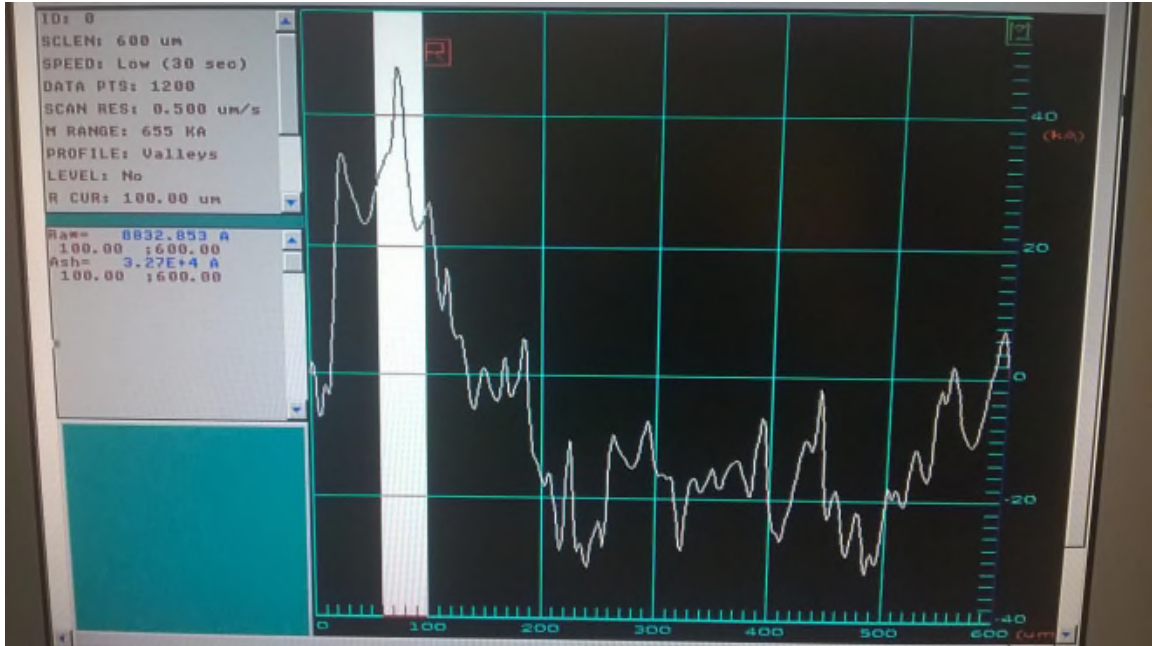
- [1] P. Campbell, M.A. Green, Light trapping properties of pyramidally textured surfaces, *Journal of Applied Physics* 62 (1987) 243–249.
- [2] A.W. Smith, A. Rohatgi, Ray tracing analysis of the inverted pyramid texturing geometry for high efficiency silicon solar cells, *Solar Energy Materials and Solar Cells* 29 (1993) 37–49.
- [3] V.K. Varadan, X. Jiang, V.V. Varadan, *Microstereolithography and Other Fabrication Techniques for 3D MEMS*, Wiley, New York, 2000.
- [4] H. Lee, S. An, E. Lee, A new method of optical interconnection for multiply stacked planar optical circuit boards using 45° reflection coupling, *Microelectron. Eng.* 87 (2010) 1336–1339.
- [5] K. Sato, M. Shikada, T. Yamashiro, M. Tsunekawa, S. Ito, Anisotropic etching rates of single-crystal silicon for TMAH water solution as a function of crystallographic orientation, *Sens. Actuators* 73 (1999) 131–137.
- [6] I. Zobel, M. Kramkowska, Etch rates and morphology of silicon (h k l) surfaces etched in KOH and KOH saturated with isopropanol solutions, *Sens. Actuators. A* 115 (2004) 549–556.
- [7] M. Shikida, K. Sato, K. Tokoro, D. Uchikawa, Differences in anisotropic etching properties of KOH and TMAH, *Sens. Actuators* 80 (2000) 179–188.
- [8] S. Chandrasekaran, J. Check, S. Sundararajan, P. Shrotriya, The effect of anisotropic wet etching on the surface roughness parameters and micro/nanoscale friction behavior of Si(1 0 0) surfaces, *Sens. Actuators A* 121(2005) 121–130.
- [9] S. Chandrasekaran, S. Sundararajan, Effect of microfabrication processes on surface roughness parameters of silicon surfaces, *Surf. Coat. Technol.* 188 (2004) 581–587.
- [10] M.A. Gosálvez, K. Sato, A.S. Foster, R.M. Nieminen, H. Tanaka, An atomistic introduction to anisotropic etching, *J. Micromech. Microeng.* 17 (2007) S1–S26.
- [11] M.A. Gosálvez, Y. Xing, K. Sato, Analytical solution of the continuous cellular automaton for anisotropic etching, *J. Microelectromech. Syst.* 17 (2008) 410–431.
- [12] Z. Zhu, C. Liu, Simulation of anisotropic crystalline etching using a continuous

- cellular automata algorithm, *Comput. Model. Eng. Sci.* 1 (2000) 11–19.
- [13] Z.F. Zhou, Q.A. Huang, W.H. Li, W. Deng, A cellular automaton based simulator for silicon anisotropic etching processes considering high index planes, *J. Micromech. Microeng.* 17 (2007) S38–S49.
- [14] M.A. Gosálvez, I. Zobel, E. Viinikka, Wet etching of silicon, in: V. Lindroos, et al. (Eds.), *Handbook of Silicon Based MEMS Materials and Technologies*, Elsevier: William Andrew, Amsterdam, 2010, pp. 375–407.
- [15] K. Sato, M. Shikida, Y. Matsushima, T. Yamashiro, K. Asaumi, Y. Iriye, M. Yamamoto, Characterization of orientation-dependent etching properties of single-crystal silicon: effects of KOH concentration, *Sens. Actuators A* 64 (1998) 87–93.
- [16] I. Zobel, M. Kramkowska, The effect of alcohol additives on etching characteristics in KOH solutions. Review, *Sens. Actuators A* 101 (2002) 255–261.
- [17] H. Seidel, L. Csepregi, A. Heuberger, H. Baumgartel, Anisotropic etching of crystalline silicon in alkaline solutions, *Journal of the Electrochemical Society* 137 (1990) 3612–3626.
- [18] I. Zobel, I. Barycka, Silicon anisotropic etching in alkaline solutions I. The geometric description of figures developed under etching Si (1 0 0) in various solutions, *Sensors and Actuators A* 70 (1998) 250–259.
- [19] T. Juvonen, J. Harkonen, P. Kuivalainen, High efficiency single crystalline silicon solar cells, *Physica Scripta T101* (2002) 96–98.
- [20] Y. Zhang, Y.Q. Zhou, Z.Y. Jiang, F.Z. Liu, M.F. Zhu, Effect of acid-based chemical polish etching on the performance of silicon heterojunction solar cells, *Physica Status Solidi C* 7 (2010) 1025–1028.
- [21] M. Shikida, K. Tokoro, D. Uchikawa, K. Sato, Surface morphology of anisotropically etched single-crystal silicon, *J. Micromech. Microeng.* 10 (2000) 522–527.
- [22] K. Sato, M. Shikida, T. Yamashiro, M. Tsunekawa, S. Ito, Roughening of single crystal silicon surface etched by KOH water solutions, *Sens. Actuators A* 73 (1999) 122–130.
- [23] M. Shikida, K. Sato, K. Tokoro, D. Uchikawa, Differences in anisotropic etching

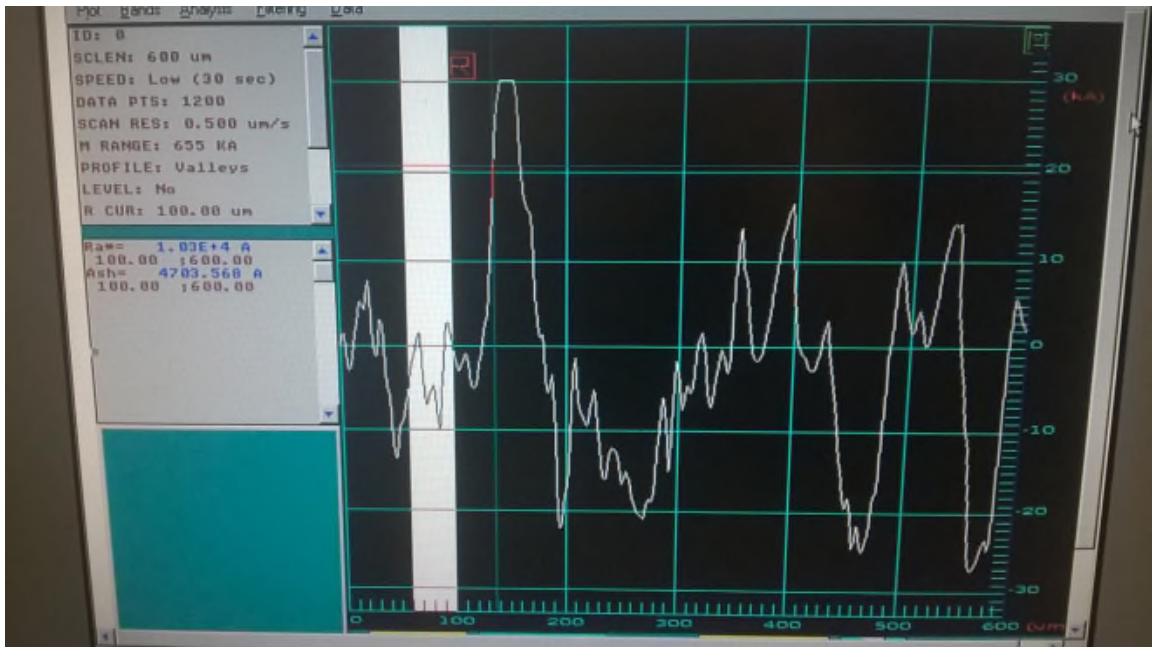
- properties of KOH and TMAH solutions, *Sens. Actuators A* 80 (2000) 179–188.
- [24] E. van Veenendaal, K. Sato, M. Shikida, J. van Suchtelen, Micromorphology of single crystalline silicon surfaces during anisotropic wet chemical etching in KOH and TMAH, *Sens. Actuators A* 93 (2001) 219–231.
- [25] J. Flidr, Y.C. Huang, Extracting site-specific reaction rates from steady state surface morphologies: kinetic Monte Carlo simulations of aqueous Si(111) etching, *J. Chem. Phys.* 108 (13) (1998) 5542–5553.
- [26] R.A. Wind, M.A. Hines, Macroscopic etch anisotropies and microscopic reaction mechanisms: a micromachined structure for rapid assay of etchant anisotropy, *Surf. Sci.* 460 (2000) 21–38.
- [27] M.A. Green, *Solar Cells: Operating Principles, Technology and System Application*, vol. 1, University of New South Wales, Kensington, 1982.
- [28] K.E. Bean, *IEEE Trans. Electron Dev.* ED-25 (1978).
- [29] D. Iencinella, E. Centurioni, R. Rizzoli, F. Zignani, *Sol. Energy Mater. Sol. Cells* 87 (725) (2005).
- [30] H. Park, J.S. Lee, S. Kwon, S. Yoon, H. Lim, D. Kim, Investigation of improving texturing effect by surface saw damage etching using acidic etchant for silicon solar cells, *J. Kor. Inst. Met. Mater.* 46 (12) (2008) 835–840.
- [31] E. Yablonovitch and G. D. Cody, “Intensity enhancement in textured optical sheets for solar cells,” *IEEE Trans. Electron. Dev.* 29(2), 300–305 (1982).
- [32] E. Yablonovitch, “Statistical ray optics,” *J. Opt. Soc. Am.* 72(7), 899–907 (1982).
- [33] A. Goetzberger, “Optical confinement in thin Si-solar cells by diffuse back reflectors,” in *Proceedings of IEEE Photovoltaic Specialists Conference (IEEE, 1981)*, pp. 867–870.
- [34] M. A. Green, “Lambertian light trapping in textured solar cells and light-emitting diodes: Analytical solutions,” *Prog. Photovolt. Res. Appl.* 10(4), 235–241 (2002).
- [35] U. Rau, U. W. Paetzold, and T. Kirchartz, “Thermodynamics of light management in photovoltaic devices,” *Phys. Rev. B* 90(3), 035211 (2014).

- [36] M. Ledinský, E. Moulin, G. Bugnon, K. Ganzerová, A. Vetushka, F. Meillaud, A. Fejfar, and C. Ballif, "Light trapping in thin-film solar cells measured by Raman spectroscopy," *Appl. Phys. Lett.* 105(11), 111106 (2014).
- [37] C. Barugkin, Y. Wan, D. Macdonald, and K. R. Catchpole, "Evaluating plasmonic light trapping with photoluminescence," *IEEE J. Photovolt.* 3(4), 1292–1297 (2013).
- [38] E. Daub and P. Würfel, "Ultralow values of the absorption coefficient of Si obtained from luminescence," *Phys. Rev. Lett.* 74(6), 1020–1023 (1995).
- [39] P. Würfel, "The chemical potential of radiation," *J. Phys. C Solid State Phys.* 15(18), 3967–3985 (1982).
- [40] T. Trupke, E. Daub, and P. Würfel, "Absorptivity of silicon solar cells obtained from luminescence," *Sol. Energy Mater. Sol. Cells* 53(1–2), 103–114 (1998).
- [41] P. Würfel, T. Trupke, T. Puzzer, E. Schäffer, W. Warta, and S. W. Glunz, "Diffusion lengths of silicon solar cells from luminescence images," *J. Appl. Phys.* 101(12), 123110 (2007).
- [42] M. Rüdiger, T. Trupke, P. Würfel, T. Roth, and S. W. Glunz, "Influence of photon reabsorption on temperature dependent quasi-steady-state photoluminescence lifetime measurements on crystalline silicon," *Appl. Phys. Lett.* 92(22), 222112 (2008).
- [43] M. A. Green, "Analytical expressions for spectral composition of band photoluminescence from silicon wafers and bricks," *Appl. Phys. Lett.* 99(13), 131112 (2011).
- [44] C. Schinke, D. Hinken, J. Schmidt, K. Bothe, and R. Brendel, "Modeling the spectral luminescence emission of silicon solar cells and wafers," *IEEE J. Photovolt.* 3(3), 1038–1052 (2013).
- [45] T. Kirchartz, A. Helbig, and U. Rau, "Note on the interpretation of electroluminescence images using their spectral information," *Sol. Energy Mater. Sol. Cells* 92(12), 1621–1627 (2008).
- [46] B. Schwartz and H. Robbins, "Chemical etching of silicon," *Journal of the electrochemical society*, vol. 123, p. 1903, 1976.

SUPPLEMENTARY DIAGRAMS

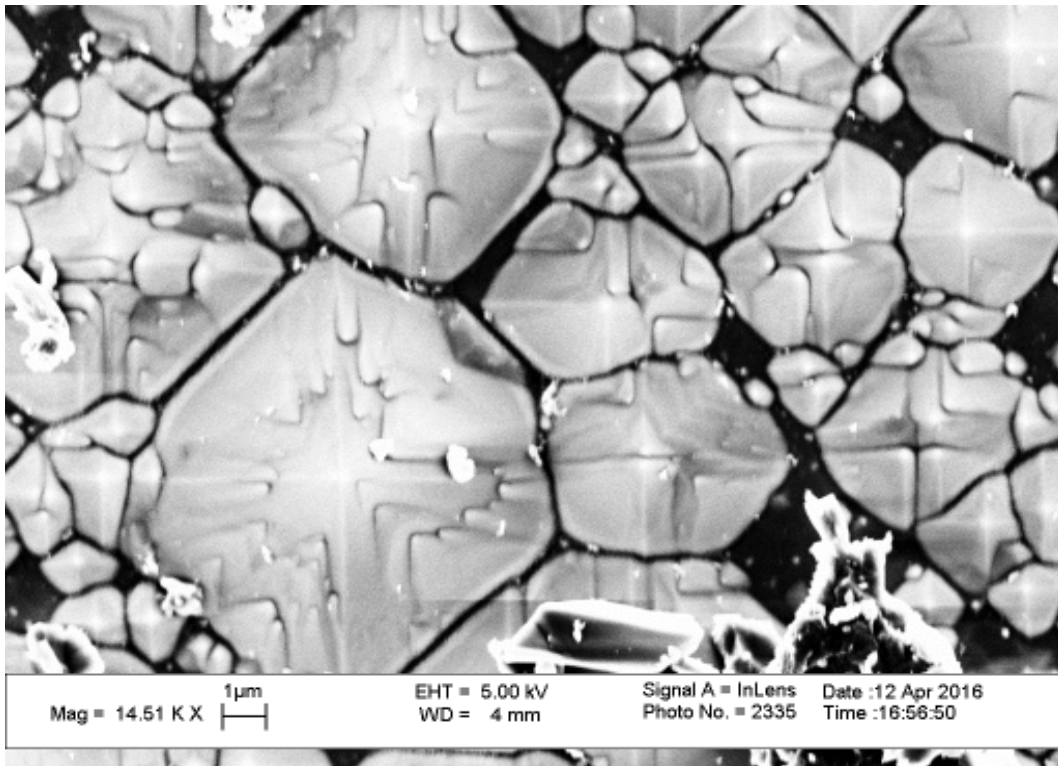


(a)

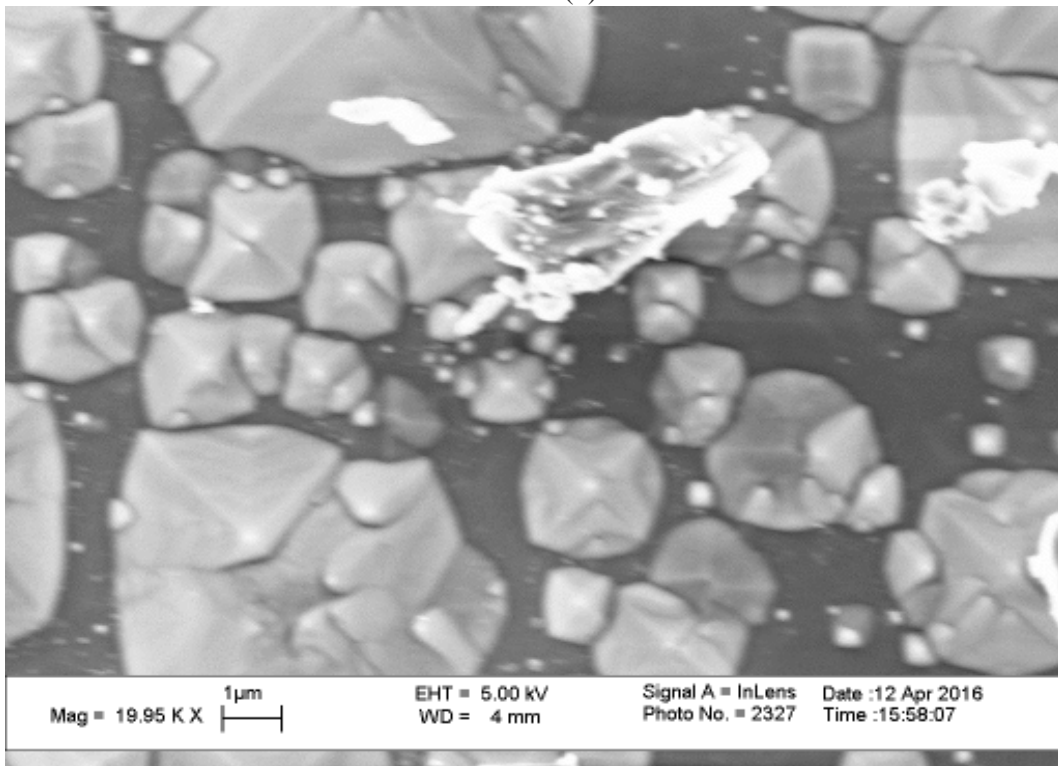


(b)

Figure 6.1 Screenshots of profilometer spectrograms of samples. (a) Sample etched in tangent position; (b) Sample etched in vertical position. All of them were etched in 1mol/L KOH solution at 70°C for 60minutes.



(a)



(b)

Figure 6.2 SEM images of etched Si surface morphology showing pyramidal and hillock structures.(a) Sample etched in 1mol/L, 70°C, 0.5h; (d) Sample etched in 2mol/L, 70°C, 1h.